ISA Transactions 120 (2022) 147–166

Contents lists available at ScienceDirect

ISA Transactions

journal homepage: www.elsevier.com/locate/isatrans

Research article

Metal-based additive manufacturing condition monitoring methods: From measurement to control

Xin Lin [a,c], Kunpeng Zhu [a,b,*], Jerry Ying Hsi Fuh [c], Xianyin Duan [a]

[a] Department of Mechanical Automation, Wuhan University of Science and Technology, Wuhan 430081, China
[b] Institute of Advanced Manufacturing Technology Chinese Academy of Sciences, Changzhou, China
[c] Department of Mechanical Engineering, National University of Singapore (NUS), Singapore

ARTICLE INFO

Article history:
Received 20 August 2020
Received in revised form 1 March 2021
Accepted 1 March 2021
Available online 5 March 2021

Keywords:
Metal-based additive manufacturing
Condition monitoring
Measurement and control
Machine learning

ABSTRACT

Compared with other additive manufacturing processes, the metal-based additive manufacturing (MAM) can build higher precision and higher density parts, and have unique advantages in the applications to automotive, medical, and aerospace industries. However, the quality defects of builds, such as dimensional accuracy, layer morphology, mechanical and metallurgical defects, have been hindering the wide applications of MAM technologies. These decrease the repeatability and consistency of build quality. In order to overcome these shortcomings and to produce high-quality parts, it is very important to carry out online monitoring and process control in the building process. A process monitoring system is demanded which can automatically optimize the process parameters to eliminate incipient defects, improve the process stability and the final build quality. In this paper, the current representative studies are selected from the literature, and the research progress of MAM process monitoring and control are surveyed. Taking the key components of the MAM monitoring system as the mainstream, this study investigates the MAM monitoring system, measurement and signal acquisition, signal and image processing, as well as machine learning methods for the process monitoring and quality classification. The advantages and disadvantages of their algorithmic implementations and applications are discussed and summarized. Finally, the prospects of MAM process monitoring researches are advised.

1. Overview of MAM process monitoring system

1.1. The MAM process and properties

Due to the fast development of materials and high-energy sources, additive manufacturing (AM) technologies have made great progress in the past decade. Among them, the metal additive manufacturing (MAM) has been one of the most important branches for its big potential in industrial applications. Like other AM processes, the MAM process is based on the discrete slicing of a 3D CAD model, and with a computer numerical control (CNC) system the material (powder or wire) is fused layer by layer by controlled high-energy sources to produce metal components [1,2]. According to energy sources and material forms, MAM processes consist of selective laser melting (SLM), electron beam melting (EBM), direct energy deposition (DED), electron beam freeform fabrication (EBFF), and wire and arc additive manufacturing (WAAM) [3]. Among these processes, the SLM and the EBM are also called powder bed fusion (PBF) process due to their usage of powder bed to distribute and fuse materials. Compared with other AM processes, the MAM builds have higher precision and density, and have unique advantages in the applications to automotive, medical, and aerospace industries [4]. Table 1 summarized the MAM processes and their corresponding building properties.

Due to the complex thermo-mechanical process, the current applications of MAM are facing severe build quality challenges such as balling [5,6], lamination and cracking [7,8], powder bed anomaly [9,10], and porosity [11,12]. Therefore, it is very important to monitor and establish the correlation between process signatures and build quality to optimize and control the building process to ensure the part quality and production efficiency.

1.2. The principle of MAM process condition monitoring

Generally, the MAM condition monitoring is a data-driven method to detect the process state and build defects in the production process. It is achieved by measuring one or several parameters related to the process (i.e. material type, energy source, scanning parameters), or by measuring some physical

* Corresponding author at: Department of Mechanical Automation, Wuhan University of Science and Technology, Wuhan 430081, China.
E-mail address: kunpengz@hotmail.com (K. Zhu).

https://doi.org/10.1016/j.isatra.2021.03.001
0019-0578/

LIST OF ABBREVIATIONS

AE	Acoustic emission
AM	Additive manufacturing
AutoE	Autoencoder
CCD	Charge-coupled device
CMOS	Complementary metal oxide semiconductor
CNC	Computer numerical control
CNN	Convolutional neural network
CT	Computer tomography
DBM	Deep Boltzmann machine
DBN	Deep belief network
DED	Direct energy deposition
DT	Decision tree
EBFF	Electron beam freeform fabrication
EBM	Electron beam melting
FEM	Finite element method
FFT	Fast Fourier transform
FNs	False negatives
FPs	False positives
FT	Fourier transform
GMM	Gaussian mixture model
GP	Gaussian process
GRU	Gated recurrent unit
IR	Infrared radiations
kNN	k-Nearest Neighbor
LR	Logistic regression
LSTM	Long short-term memory network
MAM	Metal-based additive manufacturing
MIMO	Multi-input–multi-output
ML	Machine learning
MLP	Multilayer perceptron neural network
MP	Model predictive control
NDT	Non-destructive testing
NIR	Near infrared
NN	Neural networks
PBF	Powder Bed Fusion
PCA	Principal component analysis
PID	Proportional–integral–derivative
PSD	Power spectrum density
RF	Random forest
RNN	Recurrent neural network
SIFT	Scale-invariant feature transform
SLM	Selective laser melting
SLS	Selective laser sintering
SOM	Self-organizing maps
STFT	Short-time Fourier Transform
SVM	Support vector machine
UV	Ultraviolet
WAAM	Wire and arc additive manufacturing

phenomenon [13–17], and then applied these signatures to determine the build defects and decision strategies. There are complex physical and metallurgical processes that happened in the MAM process, including heating, melting, Marangoni convection, evaporation, solidification [4,18,19]. The interactions of these phenomena produce visible and ultraviolet radiation, acoustic and electronic signals [20], and the dynamic variations of these signals reflect the changes of the current build state. Fig. 1 shows the process and mechanism of laser melting and signal generation. The radiation emission (plasma plume), laser reflection, scattering and conduction heat flow are important, the features of which provide the process quality information. A good process monitoring system can improve the manufacturing process stability and consistency, and control the final product quality as a result. For this purpose, studies are conducted and surveyed from different perspectives, such as measurement [15,16,21–24] , defect monitoring [25,26], monitoring and control [21,22,27,28] . Commercial equipment manufacturers have also developed some basic modules for melt pool monitoring [29] and process monitoring [30], which are however at the initial stage and limited in functions.

The MAM condition monitoring system can basically be divided into offline and online monitoring system. The offline monitoring is to measure the process state before and after building, which is usually applied in the initial research stage to study process phenomena and mechanics. The online monitoring is also referred to as in-situ monitoring, which intends to monitor the process state and make corresponding decision strategies upon the online measurements. Online monitoring approaches are preferred in research and applications as they help to reveal the process mechanism [21,31] and lay the foundation for control and automation [32–35], which would eventually improve the production efficiency. Online monitoring approaches have been mostly studied in recent years [15,16,27,28,36,37]. It is noted that this study does not intend to conduct an exhausting survey of all literatures. From the authors' view, we generally select the representative articles that are most associated with MAM process monitoring.

The online monitoring system is a real-time closed-loop control system, which mainly consists of AM system parameter monitoring, signal acquisition, feature analysis and defect analysis modules (Fig. 2). Based on the proper selection and installation of sensors, the signal acquisition module sends the analog signal to the data acquisition device, and converts it into a digital signal convenient for further processing; the feature analysis module conducts signal preprocessing, feature extraction and selects the sensitive feature vectors to represent AM build states. The quality analysis module finally establishes the mapping relationship between signal features and build quality to classify or predict the process states.

2. Process measurement and signal acquisition

With the complex physical–chemical interactions, MAM processes produce many kinds of signals. There are five main types of signals observed in the building process, namely, infrared radiations (IR) emitted from the melt pool, visible lights and ultraviolet (UV) emitted from the plasma, audible sounds from air, ultrasonic waves from solid structure, and electric signals from plasma. These signals can be captured with the photodiode, high-speed charge-coupled device (CCD) (camera), complementary metal oxide semiconductor (CMOS) camera, and acoustic transducer etc. These measurements are summarized in Table 2, and will be discussed in the following sections.

2.1. Optical signals

The infrared (IR) light is generated from the radiation heat accumulated locally in the melt pool [2]. The melt pool is composed of liquid metal at melting point temperature, which is the source of thermal radiation, mainly in the infrared range (700–2300 nm) [28,41]. During the coaxial monitoring and considering the limitation of the wavelength range of the laser scanner beam splitter and the processing window lens, it is more significant for

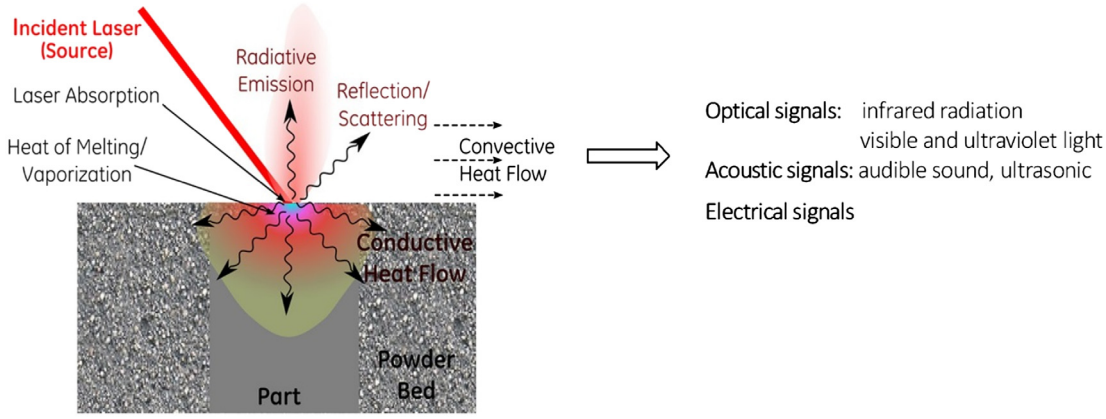

Fig. 1. Melt pool signal generation in the SLM process (the left part is adapted from [20]).

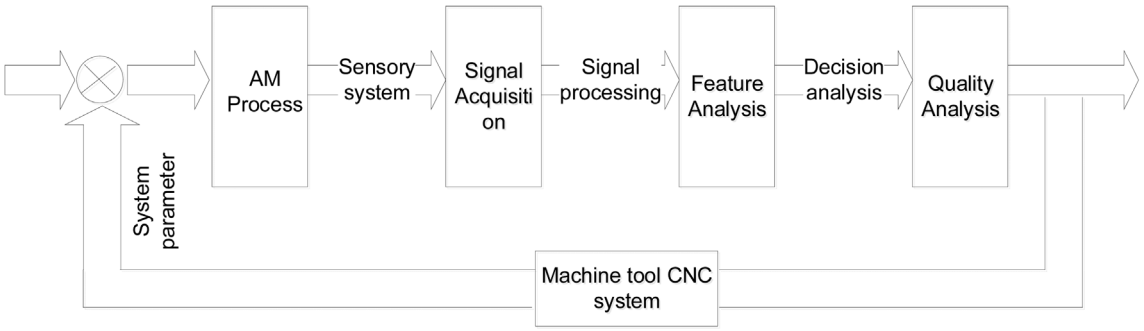

Fig. 2. The components of AM process online monitoring system.

Table 1
Comparison of technical principles and characteristics of typical MAM processes.

	SLM	DED	EBM	EBFF	WAAM
Energy source	Laser (single mode)	Laser (multi-mode)	Electron beam	Electron beam	Electric arc
Focal spot diameter	30–200 μm	0.5–3 mm	200–500 μm	1–3 mm	1-3 mm
Output power	50–1000 W	>1000 W	>2 kW	>1000 W	>1000 W
Material form	Powder	Powder	Powder	Wire	Wire
Working environment	Inert gas	Inert gas	Vacuum (10^{-4} pa)	Vacuum (10^{-4} pa)	Inert gas
Build size	Medium, small	Large, medium	Medium, small	Large	Extra large
Build accuracy	±0.1 mm	±0.5 mm	±0.4 mm	±1 mm	±2 mm
Surface roughness	Ra 6–10	Ra 20–50	Ra 20–50	Ra 20–50	>Ra 50
Post processing	Almost no	Less	Almost no	Less	Much
Processing materials	Ti, Fe, Ni, Al base alloys	Ti, Fe, Ni, Al base alloys	Ti, Fe, Ni, Al base alloys	Ti, Fe, Ni, Al base alloys	Ti, Al base alloys, steel

the signal acquisition within the near infrared (NIR) wavelength (700–1000 nm) [23]. Craeghs et al. [38–41] developed a series of monitoring and control methods for the melt pool monitoring in SLM using a combined CCD camera and photodiode optical system. By assembling a camera and a photodiode sensor in the coaxial optical path to monitor the whole melting area, a feedback control system using a CCD camera and photodiode was designed to monitor the temperature distribution of the melt pool and improve the quality of the overhanging lower surface [38]. They used a high-speed CMOS camera to measure the length, width and area of the melt pool for each threshold image, and used the photodiode to monitor the controller stability. The process parameters of laser power and scanning speed were optimized finally to obtain the builds with high density and good surface finish [39]. In addition, they also extracted melt pool properties on the horizontal plane to detect the thermal stress and suspension structure deformation caused by overheating [40]. These optical setups enabled the SLM process to record the strength, area, length and width of the molten pool, and clarified that the changes of melt pool were related to the porosity of the build [41]. These studies have made great progress in the detection of internal defects and prediction of microstructure, but there are still many limitations. As the dynamic temperature field information mainly comes from infrared or near-infrared thermal imaging, which has limited the time and spatial resolutions, the sensitivity and defect detection accuracy are not high. In addition, there is evaporation phenomenon in the melting process of SLM, and the metal vapor will cause obvious changes in the transmittance of observation window, which is detrimental to continuous dynamic temperature field monitoring.

Furumoto et al. [48] implemented a high-speed camera to monitor the melting and solidification process of metal build, with which the melting mechanism and the powder layer thickness effect were clarified. Kleszczynski et al. [49] used a high-resolution CCD camera with the off-axial observation window to visualize the process defects, and a series of measurements to reduce process faults were proposed. In addition, Yadroitsev et al. [43] measured the temperature of heat affected zone (HAZ) through an online CCD optical monitoring system, studied the temperature gradient and heat transfer process, and determined the microstructure and mechanical properties of the builds.

Table 2
The MAM process measurement methods.

Signal	Sensor	Properties monitored	Refs.	Comments
Optical Signal (infrared, ultraviolent emissions, visual light, plasma)	CCD, CMOS camera, photodiode	Melt pool dynamics and temperature distribution	[38–43]	Machine vision setup; convenient and direct observation; photo diode low accuracy and sensitivity; CCD and CMOS data high computational cost.
	Pyrometer, CCD, CMOS camera	Temperature distribution, part quality	[44–46]	
		Balling phenomenon	[47]	
		Temperature distribution, consolidation mechanism	[48]	
		Process error detection	[49]	
	Thermal imaging system, Inline coherent imaging system	process deviation detection	[50,51]	
		Part layout and gas flow effects, part quality	[52]	
		Process defects, parameter variations	[53]	
		Spatter behaviors and impacts on part quality	[54]	
	CCD, thermal camera	Plasma temperature, electron density variations	[55]	
		Temperature gradient and cooling dynamics	[56,57]	
		Keyhole formation	[58]	
Acoustic signal	Ultrasonic transducer	Surface dynamics	[59]	Ultrasonic signal: noisy, defect localization and depth; limited by the build shape; Audible signal: easy to acquire, noisy.
	Microphone	Defect correlation with process parameters	[60]	
	Spatially resolved acoustic spectroscopy	Surface and undersurface defects	[61]	
Electronic signal and miscellaneous signal	Eddy current system	Irregular porosity and delamination.	[62]	Electronic signal: device uneasy to install.
	CCD	Plasma temperature, electron density variations.	[55]	
	Thermocouple, strain gauges	Residual stresses	[63]	

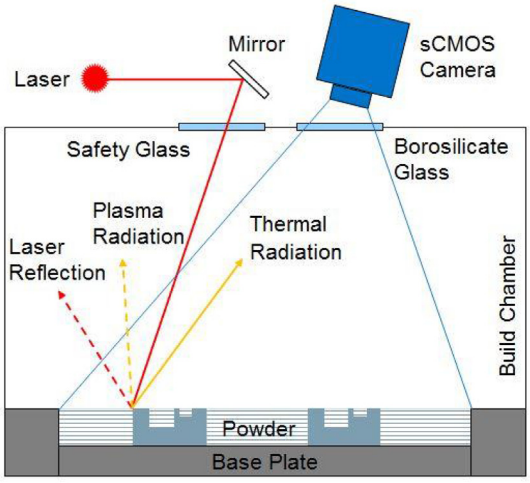

Fig. 3. The operation principle of sCMOS camera and SLM optical tomography [64].

Zenzinger et al. [64] studied the optical tomography for the SLM process monitoring. It used a 5-megapixel thermally stable sCMOS camera to capture the thermal radiation generated by the melt pool. The thermal radiation spectrum was in the visible wavelength between 380 and 780 nm. The optical setup enabled a field of view of 250 x 250 mm and a geometric resolution of about 0.1 mm/pixel (Fig. 3). The intensity and shape of the melt pool were captured by photodiodes during laser exposure. It was noted that during the exposure, the optical tomography camera needed a long time exposure to capture the melting and solidification process as well as to detect hot or cold spots (Fig. 4).

The droplet spray and powder spatter caused by the recoil pressure in the process of laser melting contain a lot of ultraviolet and visible light. Andani et al. [65] used high-speed photography to observe the spatter formation mechanism and the behaviors in SLM. An image analysis framework was developed to evaluate the size and quantity of spatter, determine the shape and composition of spatter and its impact on the surface of manufacturing parts. In the SLM process, the spectrum of plasma can be analyzed by the temperature and electron density of different melting parameters, so as to understand the influence of plasma on the process stability [55]. Liu et al. [54] used a high-speed camera to observe the dynamics of spatter with different energy inputs, and

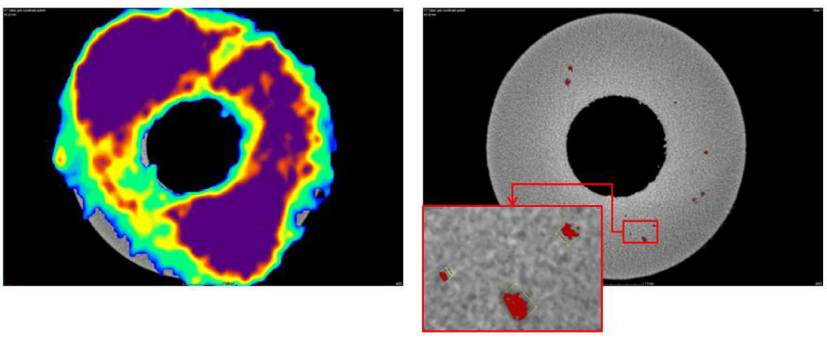

Fig. 4. Optical tomography capture single layer cold and hot area image. Left: "hot spot" optical tomography features; right: lacking fusion defects (red) [64]. (For interpretation of the references to colour in this figure legend, the reader is referred to the web version of this article.)

the results showed that energy input affected the size of spatter and spray height.

It is observed that the optical signals are mostly applied for the SLM process, and rarely used in the EBM process. This is mainly due to the difference of process nature of SLM and EBM. The optical monitoring system has high requirements for the relative position of sensor and light source, which needs to modify the building machine. As the SLM process is filled with inert gas in the chamber, the metal evaporation is effectively suppressed and the heat dissipation condition is improved. As a result, the sensor can be directly placed in the chamber to facilitate the system integration. The EBM process is carried out in vacuum environment, which has more serious metal evaporation phenomenon, higher ambient temperature and higher intensity radiation, which severely limits the application of the above detection methods.

2.2. Acoustic and electronic signal

Because of its simplicity and low cost, acoustic sensors have been widely used in MAM process monitoring. Khosroshahi et al. [66] studied the correlation between surface quality and process phenomena and frequency response of acoustic signal. This approach was listed as a potential technology to monitor the SLM process [67]. In SLM process, Ye et al. [60] found a good correspondence between acoustic signal and laser power as well as laser scanning speed. Rieder et al. [59] designed an online ultrasonic monitoring system to study the dynamics of melting process. Through the evaluation of echo signals, the residual stress was qualitatively evaluated, and the porosity could be predicted through estimating the ultrasonic velocity. Meanwhile, as the acoustic-related sensors generally capture miscellaneous acoustic information provided with enough power within the bandwidth, advanced signal processing is required to separate or filter these signals to examine the corresponding acoustic features of crack, porosity, process noise, and so on.

In the MAM process, there are electronic and other signals that can be used for monitoring, such as eddy current [62], magnetic field [67] and vibration. It has been found that the change of electrons can be used to judge the change of penetration, and with this benefit the formation of cavities can be identified and located [55]. Smith et al. utilized the acoustic wave generated by the absorbed laser heat, through the space-resolved acoustic spectrum technology, the pulse laser imaging on the structure surface, and detected the properties and defects inside and outside the layer [61]. Van et al. [63] installed pyrometer and strain gauges at the bottom of the melting platform to measure the thermal stress generated during the melting process, and used this measurement system to evaluate the maximum value and change of residual stress.

2.3. Some comments on the measurement methods

At present, most of the MAM process monitoring systems are based on optical setups and they capture the process information by machine vision. Although the visual information can explain the phenomenon of melting process directly and sufficiently, the image acquisition by high-speed camera is needed, and it causes time delay due to massive data processing. These approaches are not conducive to feedback control. Meanwhile, the one dimensional signal monitoring, i.e., acoustic signal, could be implemented conveniently by non-contact setup, and has a fast acquisition and processing speed for online monitoring. However, the one-dimensional signals can only indirectly indicate the building states in the MAM process. Therefore, the combination of heterogeneous information and the multi-sensor fusion system [68] would utilize the advantages of different sensors to conduct intelligent online monitoring of the MAM process.

3. Feature extraction

The robust and reliable mappings of the key process parameters and signatures to the quality state are most important for the MAM process monitoring. The main process parameters are laser (or electron beam) scanning parameters, powder properties, powder bed specifications, recoating system parameters. The process signatures are extracted from sensory measurements, such as plasma emission, radiation, and reflected lights. These signals usually contain heavy noise, and must be processed properly to extract the features corresponding to different process conditions and defects. The commonly used feature extraction methods are time domain, frequency domain, and time–frequency domain method [69]. Table 3 classifies and summarizes the related literatures from these three aspects.

3.1. Feature extraction based on signal processing

3.1.1. Feature extraction in time/spatial domain

The digital signal is obtained by discrete sampling and quantization of continuous sensory measurements. Generally, the time domain digital signal $f(t)$ is not directly used to determine the process state, but to extract statistical features such as mean, variance, skewness, kurtosis, peak factor etc. for further processing [70–78]. In particular, for the ith segment x_i of the signal $f(t)$, the fundamental statistics are the mean $\bar{x}$, root mean square x_{rms}, and variance X_{var} defined as follows:

$$\bar{x} = \frac{1}{N}\sum_{i=1}^{N} x_i \tag{1}$$

$$x_{rms} = \sqrt{\frac{1}{N}\sum_{i=1}^{N} x_i^2} \tag{2}$$

$$X_{\text{var}} = \frac{1}{N-1}\sum_{i=1}^{N}(x_i - \bar{x})^2 \tag{3}$$

which characterize the signal center, strength and the degree of signal deviation from the center respectively.

These statistical features are mostly applied for empirical studies of the process phenomena. The melt pool dynamics is widely studied with these features to reveal the process physics and the thermal flow during building [70–74]. It is very challenging for melt pool monitoring due to its fast elapse in a small spatial area. As a result, high speed melt pool monitoring system were developed [21,71]. In this way, the process phenomena such as melt pool shape variations [71,72], solidification and phase transformation [72] were studied and empirically described by visible and NIR emissions to indicate the build quality. Islam et al. [74] conducted a comparative study of the temperature profiles of two different setups, and found that some of the process instabilities were resulted from the energy input. Krauss et al. [75] identified that the total area was a good indicator for process parameter deviations, while the circularity and the aspect ratio could be used to detect the deviations. The absolute value of peak width indicated the existence of irregularities and defects. Additionally, by investigating the spatial irradiance distribution and the solidification evolution, defects could be identified up to a size of 100 μm. Other empirical studies were also examined on the process variations such as powder layer thickness, hatch distance and scanning strategy [76]. It showed that the temperature map of the laser impact region and thermal impact area were sensitive to the changes of the process state. With surface and under-surface defect measurements, Smith et al. [77] found that pore size remained the same for power varying from 140 W

Table 3
The common monitored signal and their features.

Information/Features monitored	Signals	Properties monitored	Refs.
Time/spatial domain (Empirical analysis; signal/image statistics)	Optical information within visual and thermal range (CMOS camera, photodiode, Pyrometer, CCD camera, Infrared camera)	Mechanical properties, surface roughness and dimensional accuracy	[9]
		Spatter tracking	[70]
		Melt pool geometries, keyhole formation	[21], [71–73]
		Balling phenomenon	[74]
		Process deviation	[75,76]
	Acoustic signal (acoustic emission, sound, ultrasonic)	Surface and undersurface defects	[77]
		Layer wise defects	[78]
Frequency Domain (Frequency statistics; FFT, PSD, Histogram)	Acoustic signal	Layer wise defects	[78]
		Surface dynamics	[79]
		Cracks and delamination	[80–82]
		Balling and overheating	[83]
		Build object, crack propagation	[84]
	Optical information within visual and thermal range	Process defects and characteristics	[85]
		Plasma temperature and electron density variations	[55,86]
		Surface defect	[87]
		Plume area, discontinuities	[88]
Time–frequency domain (STFT, Wavelet analysis)	Optical information within visual and thermal range	Thermal spatter and high temporal brightness bandwidth	[89]
		Build state, overhang and non-overhang printing conditions	[90]
		Interactions between the recoater blade and the powder bed	[91]
	Acoustic signal	Lack of fusion and balling effect	[92]
		Quality corresponded to porosity	[93,94]
		Porosity, layer quality	[95–97]
		Plasma plume oscillations	[98]
		Process instability, keyhole collapse	[99]

to 190 W, but the number of pores increased significantly with lower melting power, which reduced the overall material density.

Acoustic monitoring can detect specific properties of the MAM process, such as powder impact during building, the melting dynamics, vibration and noise of the MAM machine. Gaja and Liou [78] observed a good association between the high-energy acoustic signals and the building defects in DED, i.e. crack and porosity. The duration of high-energy acoustic signals is relatively short and can be distinguished from normal acoustic monitoring characteristics to identify cracks.

In practice, the above time/spatial domain analysis, based on the empirical amplitudes and their statistical features, is greatly affected by variation of working conditions. When the process parameters are different, these features vary significantly and they are hard to form a baseline for process monitoring. In this aspect, the features in frequency domain show more consistent properties.

3.1.2. Signal analysis in frequency domain

Fourier transform (FT) provides an effective means to extract the frequency components of the measured signal. For the signal $f(t)$, the FT $\hat{f}(\omega)$ is obtained by the inner product of $f(t)$ with a sinusoidal wave $e^{j\omega t}$ [68],

$$\hat{f}(\omega) = \left\langle f(t), e^{j\omega t} \right\rangle = \int_{-\infty}^{\infty} f(t) e^{-j\omega t} dt \tag{4}$$

The signal can be reconstructed with the inverse FT,

$$f(t) = \frac{1}{2\pi} \int \hat{f}(\omega) e^{j\omega t} d\omega \tag{5}$$

The Fourier Transform connects the signal $f(t)$ from the time domain to the frequency domain ω. To illustrate the frequency characteristics of the common aperiodic signal in MAM process, the power spectral density (PSD) is often used,

$$S_T(\omega_k) = \left| \hat{f}_T(\omega_k) \right|^2 / T \tag{6}$$

which describes the average of frequency power over a period.

Fig. 5 shows a typical acoustic emission (AE) signal during SLM process. The AE signal is heavily sampled (2000 kHz) due to its wide frequency band. The time signal Fig. 5(a) is rather constant with random noise. With the fast Fourier transform (FFT), both the signal and noise frequency characteristics arise. The noise (peaks in Fig. 5(b)) could then be filtered out by a digital filter. For the non-periodic monitoring signal over longer period, the PSD is more suitable and robust to describe the frequency content (Fig. 5(c)). Fig. 5(d) is the short-time Fourier Transform (STFT) which could describe both time and frequency properties, and will be discussed in the next section.

Studies [79–88] have shown that the build defects during the MAM process would affect the frequency component of the measured signal. The AE spectrum was found very sensitive to the changes of MAM build quality, such as crack, delamination, baling and other phenomena [82–85]. Generally, with the defects appearing, the amplitude of signal PSD increased significantly, and high peaks appeared in the higher frequency band [83]. With acoustic signal, Eschner et al. [84] applied the Fourier analysis using a 0.005-second window, with an effective range 0–1.3 MHz. To reduce background noise, a frequency mask of the background signal was subtracted from the FFT.

Kanko et al. [85] applied inline coherent imaging for the morphological-based process monitoring. The features of the powder, substrate, and track region were highlighted in the histogram (frequency bins) of the interface height and back scattering strength. The histogram was then normalized for comparison between different areas. Although these histograms exhibited similar shapes, substrates and tracks could be distinguished by their respective heights. Stutzman et al. [88] scanned the DED Ti-6Al-4V build using X-ray computer tomography (CT) to study defect density and localize the defect. Three measurements were studied on the reconstructed CT scans: line-to-continuum ratio around 430 nm, around 520 nm, and the total plume area. In a fixed constant laser power, an increase in defect density (due to powder flow rate or hatch pattern variations) were accompanied

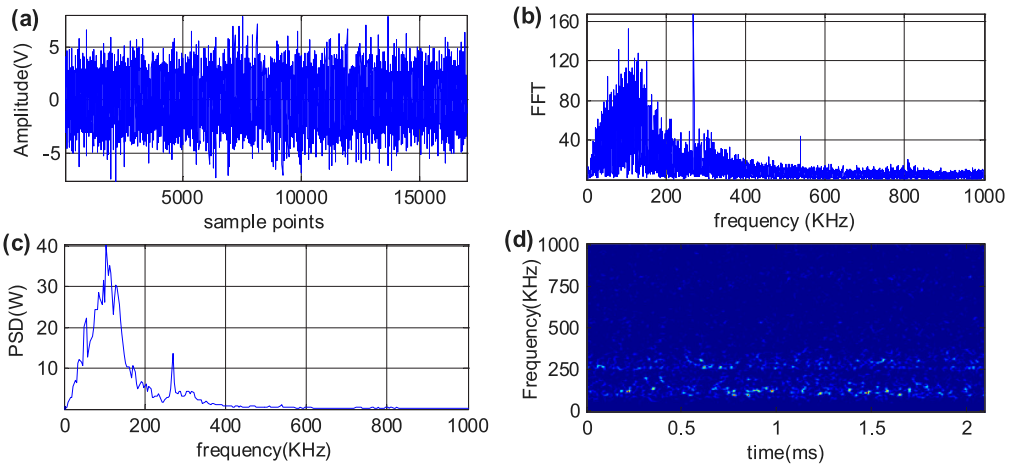

Fig. 5. The time signal (a), FFT (b) the power spectrum (c), and the STFT (d) of the AE signal in SLM process.

by an increase of these three indicators. The plasma is generated during the physical–chemical transition during the melting, which is good indication of instantaneous building state. With the plasma spectrum, the results in micro selective laser sintering (SLS) [55] showed that with the increase of the Q-switching rate from 5 to 35 kHz, the plasma temperature decreased from 9600 to 9000 K when the laser duration Q-switching was fixed. While the spectrum analysis could extract more stable information of the quality issues, its loss of local (time) information makes the frequency analysis, in most cases, only a supplementary tool for the process monitoring.

3.1.3. Time–frequency analysis

The Fourier spectrum analysis plays an important role in stationary signal analysis, while the measurements in the MAM process are mostly non-stationary. When an instantaneous detection is required in the process, the Fourier transform analysis is insufficient to describe the localities of the signals. This drawback of Fourier transform can be observed from Eq. (4): the support of $e^{j\omega t}$ expands the whole space, i.e. the $\hat{f}(\omega)$ counts on the value of $f(t)$ for all times $t \in (-\infty, \infty)$, which makes it difficult to analyze any local property of $f(t)$ from $\hat{f}(\omega)$. To this end, a sliding window function $g(t)$ is introduced with translations in time u and frequency ξ to obtain a localized time–frequency atom ϕ:

$$\phi_{u,\xi}(t) = e^{j\xi t} g(t-u) \tag{7}$$

The resultant transform is called the short-time Fourier Transform (STFT) [68]:

$$(STFT)(f(t)) = \langle f(t), \phi_{u,\xi} \rangle = \int_{-\infty}^{\infty} f(t) g(t-u) e^{-j\xi t} dt \tag{8}$$

The corresponding power $|STFT(f(t))|^2$ is called spectrogram (Fig. 5d), which is widely applied in joint time–frequency analysis. The spectrogram was applied to monitor melting pool and thermal spatter [89], overhang printing conditions [90], the interactions between the recoater blade and the powder bed [91]. It is noted that the eigen-spectrum of the spectral graph Laplacian matrix were used as signatures [90], where the graph Fourier transform skipped the intermediate signal filtering steps.

In MAM process condition monitoring, acoustic emission has been one of the most studied non-destructive testing (NDT) technique due to its sensitivity and easy implementation [92–100]. Kouprianoff et al. [92] applied AE to determine lack of fusion and balling effect of the single track. By using STFT it could clearly distinguish when scanning started and when each track was being scanned. Shevchik et al. [93,94] showed the AE signal spectrogram features were discriminative to different quality layers produced with the optimal process condition, which corresponded to the relative energies of the narrow frequency bands. Fisher et al. [100] showed that a notable difference could be obtained from the acoustic signatures of varying laser powers during SLM. A brief assessment of the capability of in-situ NDT during AM was carried [95] and reviewed [96].

Compared to fixed time–frequency resolution of STFT, wavelet transform has adaptive time–frequency positioning capability, and is more powerful in processing non-stationary signals. The wavelet transform of signal $f(t)$ is,

$$WT_f(a,\tau) = \frac{1}{\sqrt{a}} \int_{-\infty}^{\infty} f(t) \psi^* \left(\frac{t-\tau}{a} \right) dt \tag{9}$$

where $\psi_{a,\tau}(t) = \frac{1}{\sqrt{a}} \psi(\frac{t-\tau}{a})$ is a family of wavelet functions obtained by the scaling and translation of the mother wavelet $\psi(t)$. With the variations of scaling factor a and translation factor τ, the wavelet transform can provide adaptive time–frequency resolutions of the signal, which meet the signal analysis requirement. This benefit makes the WT popular in extracting important local time–frequency features in the applications.

Wasmer et al. [97] studied the AE signals by wavelet analysis and showed that there was a certain correlation between the AE signal and the build porosity. With optical emissions, wavelet analysis could identify the plasma plume oscillations [98], process instability and keyhole collapse [99]. The wavelet spectrograms were applied as a input for spectral CNN (convolutional neural network) classifiers to search for different time–frequency features [93]. It was formed by the relative energy of the narrow bands extracted from the M-band wavelet, with which multiple wavelets were applied to different signal subspaces to ensure the translation invariance. The relative energy was defined to track the redistribution of energy among different bands,

$$\rho_{norm(j,n)} = \frac{E_j(n)}{E_{total}} \tag{10}$$

where $E_j(n)$ is the wavelet coefficient energy of a specific frequency band at scale j, n, and E_{total} is a summation of the energies of all frequency bands. Fig. 6(c) showed a deprecating example in which the spectrogram was reconstructed from the pattern of the signal in Fig. 6(a) that was qualified by the red solid marker.

These data-oriented studies involve experimental measurements and large-scale numerical simulations, which results in the large amounts of data storage and computation. Salloum et al. [101] addressed this challenge by applying the wavelet

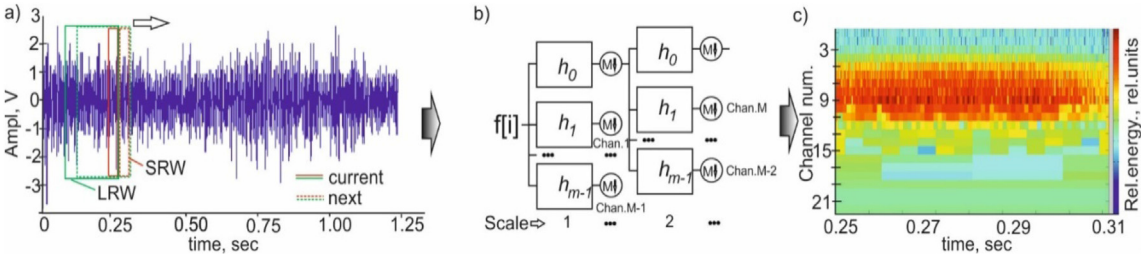

Fig. 6. (a) Typical AE signal from one complete layer of a high quality (79 J/mm^3, 500 mm/s). SRW and LRW are the short and long running windows. (b) Multiscale extraction of frequency information by M-band wavelets. (c) Reconstructed spectrogram from the relative energies of the M-band wavelets [93].

tool for compression. The results showed that the single wavelet base had the best compression performance, and the Alpert tree wavelet compression was a promising method to reduce the data size. To overcome the limitation of WT on cascade decomposition of half low-band only, wavelet packet decomposition (WPD) was developed to decompose the high frequency part which was not further decomposed by WT. In this sense, the WPD is an overcomplete representation, and the optimal wavelet packets could be selected by using the Shannon entropy criterion [102]. Researches have shown that the fusion of different domain signal features can improve the accuracy of AM state monitoring [88,89]. In many cases, the statistical characteristics of signals in the time, frequency and the time–frequency domains are combined to provide more information for a more reliable detection of the build defects.

3.2. Feature extraction based on image processing

3.2.1. Machine vision system for AM monitoring

Digital cameras are widely used in MAM process monitoring, and are mostly applied for the melt pool and powder bed anomaly detection. In particular, the PBF process enables two main sensing configurations, namely, the coaxial sensor which uses the light path of the laser to monitor the nature of the melting pool, and the off-axial sensor which allows additional amounts to be measured by larger field of view and different spatial/time scales. Craeghs et al. [103] designed an off-axial digital camera to detect the wear and local damage of the recoating blade. As shown in Fig. 7, the field of view was the build platform, and to minimize the perspective error in the image, the optical axis of the camera was chosen close to the center line of the build platform. Three light sources were used to illuminate the build platform from three directions: front lamp (perpendicular to the powder spreading motion), side lamp (parallel to the powder spreading motion) and ceiling lamp (perpendicular to the build platform). As some defects could only be seen by lighting in a certain direction, different directions were used to form a clear defect monitoring image in the powder bed.

Aminzadeh [104] proposed a machine vision framework and applied image processing algorithms to detect geometric errors and porosities of the build. In a subsequent work [105], they used a 9 megapixel visual camera mounted inside the build chamber to provide high resolution images (7 μm/pixel) and to enhance the contrast between the powder and fused regions. The resulted 80 μm detection error was less than the laser scan diameter. Kleszczynski et al. [9] applied a 29 megapixel CCD camera and active lighting to detect EBM super elevation defects, which area might collide with the recoating system. The resolution range was 20–30 μm/pixel, and the field of view area was about 150 mm × 110 mm. It extracted the super-elevation area of each position in each layer image from the detection mask, and then determined the threshold of the critical elevation region of each position according to the vibration measurements. In the subsequent effort, the authors used their imaging system with resolution 24 μm/pixel to check the height of the parts [10,87]. They took camera images from the deposited powder layer and applied a fixed threshold to detect the raised area, while the authors did not perform further analysis to verify the quality of the builds.

In MAM, the quality of the build is greatly affected by the fusion quality and porosities. The automatic detection of layers with low fusion quality or pores is important to assure the quality of final part. On the other side, sometimes the layer becomes defective due to the oscillations of laser (electron beam) parameters or local changes in thermal conduction caused by the build geometry variations [103]. Therefore, identifying incipient defects layer-by-layer would be more effective for the MAM process monitoring.

The machine vision setups can solve the MAM quality monitoring problem to some extent, but the monitoring systems are generally limited in the capability to represent 3D structures with high spatial resolution in a relatively large area (up to several square centimeters). The issues on the optimal selection of optical sensors, sensing accuracy verification, and the chosen of their corresponding spatial and temporal resolutions are still to be studied to validate these methods.

3.2.2. Visual feature extraction

Visual-based feature extraction is the process of mapping the lower-level image pixels to distinguishable upper-level numerical vectors (or semantics). In the monitoring process, the region of interest (ROI) needs to be located and segmented, and then sensitive features can be extracted. Image segmentation is vital to the object detection and defect localization [106,107]. The most common segmentation approaches are grayscale thresholding, edge detection, matching, and region growing [108]. These include the IsoData algorithm [109], Otsu's method [110], Hough transform, minimum cross entropy [111], fuzzy thresholding [112], and k-means thresholding [107].

Fig. 8(a) showed the sequence of operations to segment the images and extract the ROI [113]. The two major steps involved image thresholding and the classification of the connected components. Fig. 8(b) showed the results of an infrared image thresholding, where left-to-plume emission was clearly visible. Under the optimal threshold T, all the segmentation methods provided rather similar results.

After the segmentation, the visual properties of images, such as pattern features, shape features and color features can be extracted. Pattern features describe objects by calculating the distribution of gradient intensity and direction on the spatial area. The most widely used gradient feature was the scale-invariant feature transform (SIFT) proposed by Lowe [114], which obtained gradient information near specific key points to describe the image, enabling excellent scale and rotation invariance. Other methods like, gradient location orientation histograms, speed-up robust features, and PCA-SIFT [115] were also developed.

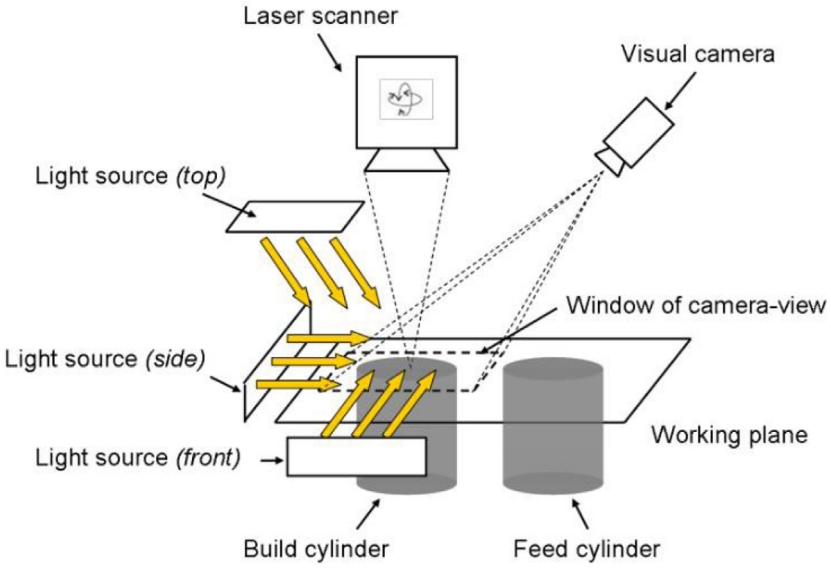

Fig. 7. Principle of visual monitoring system for top surface of powder layer [103].

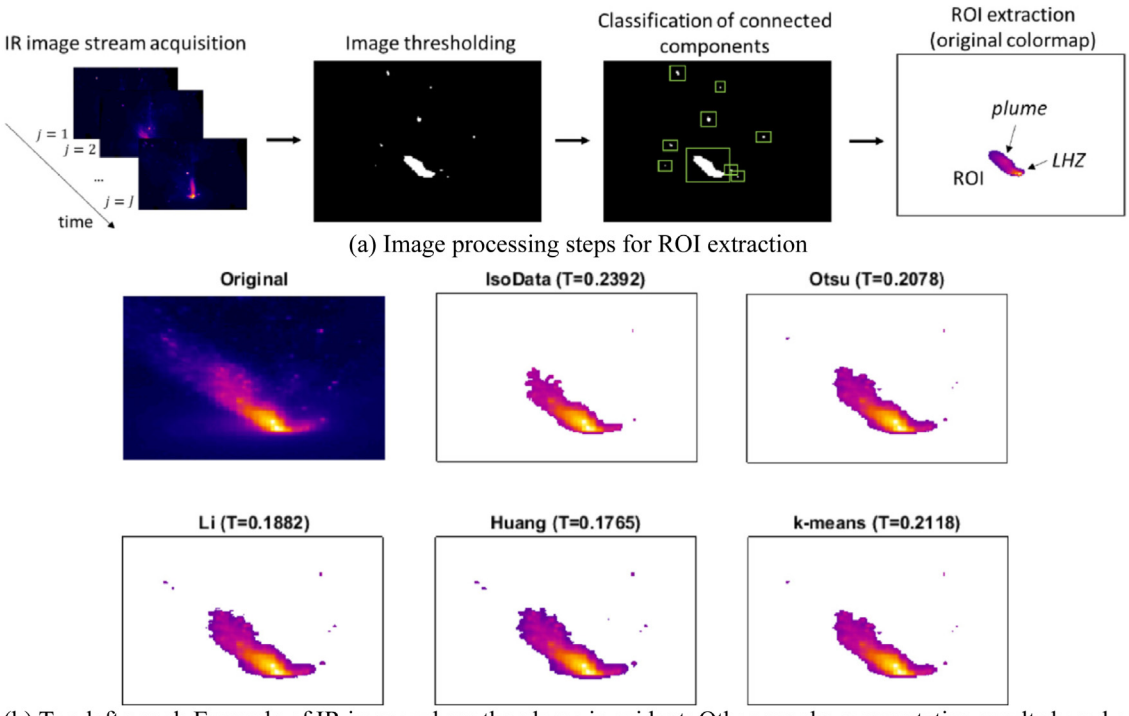

(a) Image processing steps for ROI extraction

(b) Top-left panel: Example of IR image where the plume is evident; Other panels: segmentation results based on IsoData, Otsu's, Li's, Huang's and k-means methods

Fig. 8. Visual feature extraction for SLM process monitoring [113].

The shape feature is used to describe the object contour. The common shape features are shape context, k-adjacent segmentation, convex hull, scale invariant shape features, etc. [104]. Shape features have excellent affine invariant properties, but their performance largely depends on preprocessing steps such as boundary detection and segmentation. Color feature is extracted by calculating the probability distribution of local image attributes (gray, color, etc.), which mainly includes color SIFT feature, color co-occurrence matrix, color self-similarity [106]. However, color information is instable and limited in the MAM application, for example the color features are not suitable for infrared image processing. These image feature descriptors and their performances were comprehensively evaluated for object classification [116].

The literatures [9,10,87,117–121] stated that layered imaging in PBF could be used to detect in-surface and out-of-surface profile defects, powder contaminations and powder recoating errors. More recently, methods were developed for automatically extracting features that represent changes in local surface to identify defects or abnormal melting conditions [122,123]. With these results, it should be noted that because deformations caused by shrinkage and thermal stress cannot be captured layer-by-layer, and as a result the part dimensions and geometry monitored do not necessarily represent the final quality.

In the practical monitoring process, if a significant deviation from the intended shape is observed in a layer, it may represent a defect that cannot be recovered as the building process continues. In this case, the image segmentation and the in-situ profile recognition are key issues to identify defects and deviations from the known baseline. It was also showed [124] that the image pre-processing and segmentation improved the measurement repeatability significantly.

The elevated area in the production layer brings risk of process instability as it would lead to the collision between the powder coating system and the build. Jacobsmuhlen et al. [10] trained an image classifier-based elevated area detector to identify this problem. They obtained two high-resolution images of the layer: one after the laser exposure and the other after the next layer of powder deposited. Dense descriptors were extracted and compared on their predictive capability, and the parameters were finally optimized through cross-validation of 281 images.

Researches have shown that the fractal dimension can effectively capture the change of image appearance. The optical image multifractal analysis was applied to discriminate process deviations [125]. It quantified and detected the onset of porosity due to deviation of process conditions, i.e., the occlusion of the optics due to vaporization of the material during melting and its eventual condensation. In another study, Yao et al. [126] investigated three types of defects, namely balling, crack and porosity of direct laser sintering process. The results were based on the assumption that the variations of these defects would lead to the changes of AM image contour, and influenced the image's multifractal spectrum. As shown in Fig. 9(a), three types of simulated defects were studied, which represented the possible results of balling, crack or porosity. It was noted in the fractal spectrum (Fig. 9(b)) that the image without defects had a shorter right tail than those with defects. In addition, the spectrum of balling defects had the longest right tail, while the pore defects had a relatively short tail in the fractal spectrum. In all cases, the fractal spectrum maximum was approximately 2.09763. It should be noted that the multi-fractal analysis focuses on nonlinear patterns (i.e. irregularities, singularity) of the image, rather than the single fractal dimensions of the crossing scale invariant features. These results also indicate that the dimension of a single fractal is not enough to represent the defects in CT images.

The difficulty of using visible light to monitor the melting layer lies in the analysis and processing of the captures images (mostly in gray-scale). At present, the contour extraction and defect recognition have been realized, but most of the approaches apply the offline processing mode, and the in-situ/real-time monitoring capability is far from satisfactory. On the other hand, the output of low coherence interference imaging and CT is the height distribution of the melting layer, which speedups the data analytics, but it needs to scan point by point or line by line and increases the time cost of MAM process. In addition, the analysis and interpretation of optical images need further investigation. For example, some optical images (e.g., the electron optical image) are not sensitive to the macro morphology, such as texture, roughness and so on. More researches are to be conducted on the study of macro morphology.

The above artificial designed feature is good to utilize the prior knowledge and is relatively easy to achieve, but it largely depends on the empirical acquisition of domain expert knowledge, which may not be accessible in practice. On the other side, the machine learning-based feature representation can automatically learn from the samples to represent the essential features, and shows great prospects for the feature extraction. This is to be discussed in the next section.

4. Machine learning base MAM process monitoring

The above manually designed features are a good way to utilize empirical knowledge. These methods are relatively easy to implement for feature extraction, detection and decision tasks, but they rely heavily on experiences. On the other hand, the learning-based feature expression is achieved by designing intelligent models and optimization algorithms, so that the machine automatically learns from the samples to characterize the essential characteristics of these samples. Typical approaches are shallow machine learning methods such as conventional neural networks (NN), support vector machine (SVM), Gaussian process (GP) [127], and the latest developments of deep learning methods such as convolutional neural network (CNN), deep belief network (DBN) and long short-term memory (LSTM) network [128]. Some of the NN based approaches were surveyed for additive manufacturing applications [129]. The machine learning based MAM process monitoring approaches [130–162] are summarized in Table 4.

4.1. Shallow machine learning based process monitoring

After obtaining the feature vectors of various measurements, the shallow machine learning (ML) models such as multilayer perceptron neural network (MLP) and SVM are established and trained to build the mapping between the features and process states. Sometimes the process parameters are also directly used as features for the inputs of the ML models. Early studies were focused on supervised NN for selective laser sintering (SLS) process monitoring and optimization [130–132]. Shen et al. [130] predicted the part density by NN in which the process parameters such as laser power, scan speed, scan spacing and layer thickness were used as inputs. Rong-ji et al. [131] developed an NN approach for parameter optimization so as to minimize the build shrinkage. The process parameters included laser power, scanning mode, hatch distance, laser parameters, and layer thickness. Similarly, a three-layer NN was developed to study the shrinkage behavior of SLS specimens [132], which consists of five neurons of process inputs, one neuron of shrinkage output, and twelve neurons of hidden layer. More recently, the SLM process was studied with NNs [133–138]. Marrey et al. [134] applied an MLP model to optimize the SLM process. The inputs included the process parameters (laser power, scan speed, hatch space, and beam diameter) while the outputs were ultimate properties of the build (mechanical properties, density, surface roughness, dimensional accuracy, and building time). Development of this multi-input/output MLP function leads to an intelligent system capable of controlling multiple parameters simultaneously. It is noted that a deep NN approach was claimed to classify melt pool images [133], while this approach was essentially a conventional MLP model with more hidden layers. Eschner et al. [135] evaluated different process qualities of cubes with different MLP networks with extracted acoustic signatures. The experimental validation showed the MLP could reach a classification rate over 90%. More studies were reported with MLP for monitoring trace geometry [136], melt-pool [133,137], and porosity [135,138].

Capturing the similarity among melt pool images is important to determine the melting quality but is challenging due to the varied melt pool geometries and massive data processing inefficiency. To meet these challenges, Khanzadeh et al. [137,138] transformed the ill-structured melt pool images into continuous thermal distribution models, and then clustered the thermal distributions with self-organizing maps (SOM), with which the melt pools of the same group shared similar distribution and produced similar microstructure (Fig. 10). Results showed that the SOM approach could identify the location of porosity successfully, and

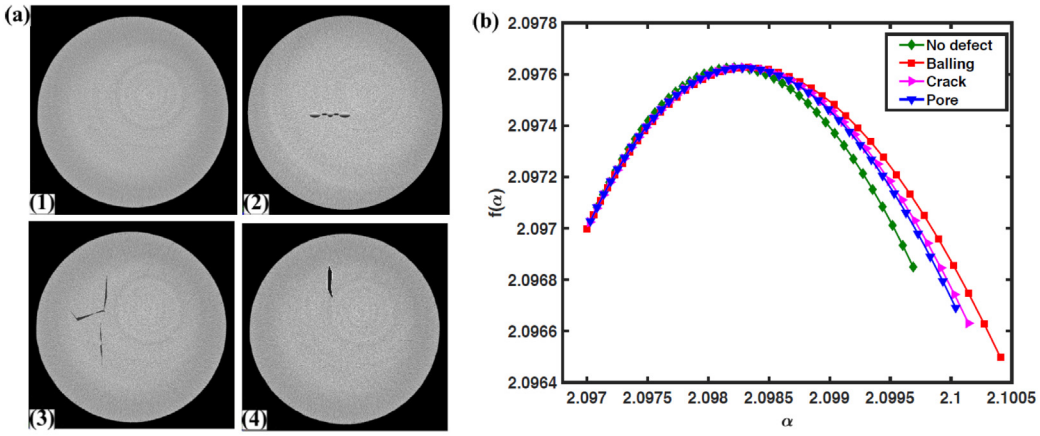

(a) AM Image contour with 1-no defect, 2-balling, 3-crack, 4-porosity; (b) multifractal spectrum of each image in (a)

Fig. 9. Multifractal analysis of image profiles for defect detection [126].

Table 4
The MAM quality monitoring with machine learning based methods.

ML method	Process	Defect/output	Refs.	Comments
Neural networks	SLS	Density, shrinkage	[130–132]	Advantages: nonlinear mapping with high precision; high classification accuracy; strong learning ability; noise robust. Disadvantages: many hyper parameters to select and learn; long learning process; local minimum, black box for the intermediate results.
	SLM	Melt-pool, Porosity, mechanical properties, dimensional accuracy	[133–135]	
	DED	Trace Geometry, melt pool and porosity detection	[136–138]	
Support vector machine	SLS	Density	[139]	Advantages: good adaptability and generalization ability; good for high dimension and small samples problems. Disadvantages: hard to train and explain; nontrivial in choosing kernel function; not suitable for large data sets.
	SLM	Melt pool, plume and spatter	[140]	
		Balling, porosity, under-melting	[141]	
		Part discontinuities	[122]	
	DED	Layer-wise quality	[142]	
Miscellaneous pattern recognition methods	DED	Cracks, porosity	[143,144]	Advantages: problem-oriented, direct, simple and effective; good results for specific problems; mostly based on (probability) distance similarity function. Disadvantages: hard to generalize; comprehensive results comparison needed; lack of complementarity.
		Operational process conditions	[80]	
		Unstable melting conditions, local defects	[113,145,146]	
		Build Finish/failure	[147,148]	
	SLM	Layer-wise anomaly detection	[149]	
		Melt pool and spatter	[150,151]	
		Overhang build	[90,125,152]	
Convolutional neural network	SLM	Porosity, part quality	[83], [153]	Advantages: Decrease of training parameters; strong learning and generalization ability; outstanding classification results. Disadvantages: need large training samples, gradient vanishing or explosion in learning; poor identification of spatial relations; low recognition ability after object rotation.
		Layer-wise defects	[154,155]	
		Overheating, balling, surface quality	[156,157]	
		Incomplete spreading, recoater hopping, part damage	[91]	
		Melt pool, plume, spatter	[140]	
		Track continuity	[158]	
		Melt pool	[159]	
	DED	Build distortion	[160]	
Deep belief network	SLM	Balling, overheating, plume, spatter	[81], [161]	Advantages: good similarity of the same class; translation invariance. Disadvantages: unsupervised learning; common classification accuracy; high learning complexity.
Recurrent neural network	DED	Thermal history	[162]	Advantages: long short-term sequence content modeling; improvement of recurrent learning. Disadvantages: many parameters to learn; image modeling inefficiency.

the inclusion of thermal distribution significantly improved the porosity prediction accuracy.

Support vector machine (SVM) is another popular ML method for process monitoring. It is a binary supervised classification method based on the Vapnik–Chervonenkis (VC) dimension theory and structural risk minimization principle [127] with which it maximizes the class margin for pattern classification. It has advantages in classifying less labeled and higher dimensional data. The SVM based methods were applied to detect part discontinuities [122], part density [139], plume and spatter evaluation [140], balling and porosity [141]. Classification of the melt pool morphologies (i.e. fingerprints) was performed using a multi-class SVM [141]. Upon the training of the model, the melt pool images captured during the overhang experiment could be classified as one of five melt pool types: desirable, balling, under-melting, keyholing porosity, or spatter. The multi-modality fingerprint was calculated and classified by the trained SVM. The multi-class SVM was able to properly delineate the fingerprints contained within the training database with an accuracy of 85.1%. It was noted that this measure of classification accuracy was not an indicator of overall algorithm performance, but only reported to demonstrate adaptability of the SVM. Seifi et al. [142] developed an SVM-based online layer-wise quality prediction method which incorporated of the tensor decomposition of melt pool images of the entire

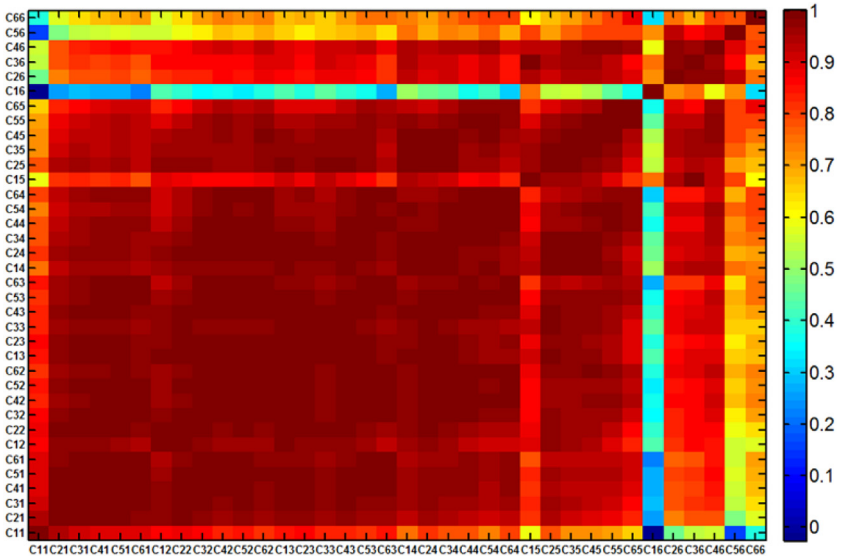

Fig. 10. Correlation matrix showing how pores were identified with melt pool thermal profile for the 36 clusters of the 6 x 6 SOM map [137].

Table 5
Performance of the four competing classifiers [149].

Method	Spatial detection			Independent detection		
	Error rate	FPs	FNs	Error rate	FPs	FNs
LR	**0.04**	2.00	**1.00**	0.13	8.00	2.00
kNN	0.09	**0.00**	7.00	0.08	0.00	6.00
SVM	0.05	1.00	3.00	0.16	6.00	6.00
RF	0.09	**0.00**	7.00	0.12	2.00	7.00

layer. This would be helpful for applying the linear SVM methods to deal with multi-dimensional and nonlinear measurement features in real applications.

Mahmoudi et al. [149] modeled spatial dependence using a GP model, and then employed a statistical test to detect significant deviations in spatially correlated images. Four standard classifiers, logistic regression (LR), SVM, k-Nearest Neighbor (k-NN), and random forest (RF) were implemented to obtain predictions for the classes of the 75 test ROIs. Table 5 summarized the results for the four classifiers in terms of the classification error rate, number of false positives (FPs), and number of false negatives (FNs), for the two scenarios of Spatial and Independent Detection. Upon inspecting Table 5, it appeared that LR outperforms the other four classifiers in terms of the classification error rate and FNs.

Many other shallow ML approaches are also developed to meet specific defect detection needs, such as logistic regression (LR) [143,146,149], k-means clustering [145], decision tree (DT), discriminant analysis [144], k-NN [144,147], Bayes classifier [147], Gaussian mixture model (GMM) [148], Gaussian process [149,151], principal component analysis (PCA) [150], and manifold learning [152]. Their applications are summarized in the first half of Table 4.

The premise of accurate condition monitoring is to extract as much effective information as possible from the massive monitoring data, but the shallow ML methods rely on a large number of signal processing technology and expert knowledge. For the processing of massive monitoring data of complex MAM process, these methods are severely limited. Deep learning methods can overcome such problems to some extent, and are powerful in handling big data with deep structural networks, which are to be discussed in the next section.

4.2. Deep learning based process monitoring

Originated from the neural network theory, deep learning methods reduces the human intervention in the feature extraction and classification, and has strong capability in learning the essential characteristics of data from large and complex sample sets. In the deep network, the original samples (measurements) are gradually transformed into features closely related to the build state, that is, the "low-level" samples are transformed into "high-level" feature expression. Compared to the shallow ML models, the DBN, deep Boltzmann machine (DBM), autoencoder (AutoE), and CNN constitute the fundamental models during the early development of deep learning [128]. Many subsequent studies are based on the modification or combination of these models. For example, the recurrent neural network (RNN) and its derivatives such as LSTM and gated recurrent unit (GRU), can deal with the problems of back-and-forth correlation between those inputs by introducing directional loops and having a deep structure in the time dimension. The network structure varies according to the number of layers, weight sharing, and edge characteristics. The majority of deep learning algorithms are embodied in the deep structure of spatial dimensions and belong to the feedforward neural network.

Shevchik et al. [153] applied the CNN with the acoustic emission for SLM in-situ quality monitoring. The monitoring approach was shown in Fig. 11. It defined low, medium and high quality, characterized by build porosity degrees. Acoustic features were extracted from all signals by the relative energy of wavelet packets. A classifier based on spectral CNN was trained to distinguish acoustic features of different qualities, where the Laplacian graph was calculated for the whole input feature space. The spectral CNN for classification computed four convolution layers, alternating with four pooling layers. The output of the structure was further transmitted to the full connection layer where the features were classified, and the results were observed in the output layer. The classification rate was between 83% and 89%. More CNN models were adapted to classify layer-wise defects [154,155], overheating, balling, surface quality issues [156,157].

Due to the dynamic nature of PBF process, the plume and spatter orientation changes according to the melt pool variations. As a result, the temporal information is an important indication of melting quality. The built quality not only depends on the current melt pool status, but also depends on the melt pool status

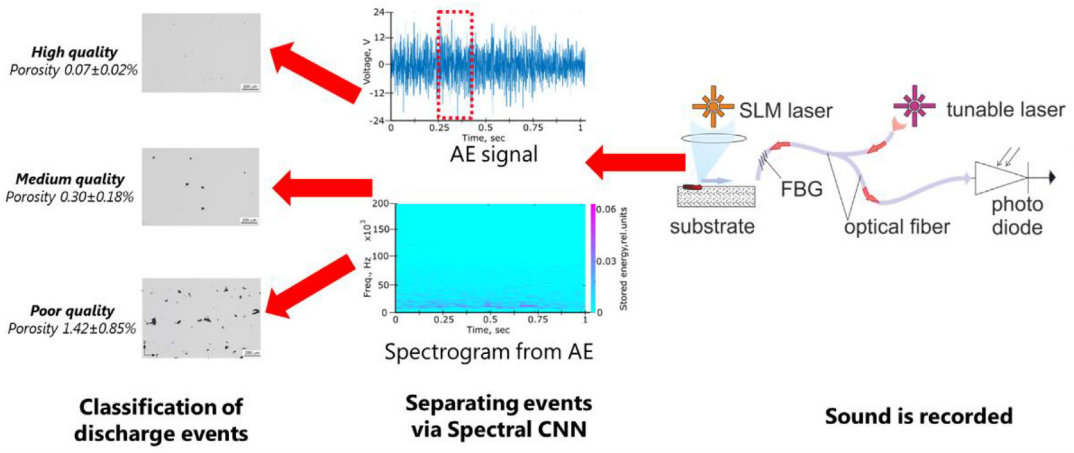

Fig. 11. The acoustic emission based spectral CNN [153].

in the next several time sequences. To this end, a hybrid CNN method [157] was proposed to learn both the spatial and temporal representative features from the raw images. It consisted of two CNN models, with the first CNN model for learning the spatial features and the second for the build quality estimation (Fig. 12). The results demonstrated that the overall classification accuracy could reach as high as 0.997 for the four process states, i.e., overheating, normal, irregularity and balling. In addition, temporal information (i.e. melt pool, plume and spatters) was identified by the CNN models. Kunkel et al. [159] applied the CNN approach to recognize melt pool images, and the model successfully classified 9280 unseen layer images by 98.9% accuracy, showing high potential for quality monitoring. Many more deep learning approaches were developed for process monitoring with CNN [83,91,140] for porosity, balling, plume and spatter [153–160], DBN for overheating, balling and spatter [81,161], and RNN for build thermal history [162]. The last part of Table 4 summarized the literatures of deep learning approaches with application to quality monitoring.

For the current condition monitoring research, a large number of deep learning models have been developed, but most of them are the superimposition of the basic models (e.g. AutoE, RBM). This form of combination often cannot take full advantages of deep learning. More effective integration of deep learning models should be studied to utilize the benefits of different deep learning approaches. To address the lack of labeled sample problem in the practical training, it would be helpful to combine the active learning or semi-supervised algorithms with deep learning methods. Additionally, the interpretability of the models and the results also need further elaboration.

4.3. Some comments on the machine learning based monitoring approaches

The machine learning based process monitoring approaches not only extract the characteristic information of the MAM process measurements, but also describe the nonlinear relationship between the monitoring data and the process state for the defect monitoring and quality prediction. However, the current ML based quality monitoring methods are purely data-driven models, and to realize closed-loop control it is necessary to fuse physical models with ML model for better performance. Meanwhile, the current complex MAM equipment is often composed of multiple interconnected components, and these components often mutually affect the process state. For example, the SLM system consists of many mechanical and electronic subsystems (such as powder beds, coating subsystems, feeding systems, etc.), while the machine learning-based monitoring methods do not model the interactions. How to model these multi-mode interactions with machine learning approaches also needs further investigation.

5. The control of MAM process

5.1. The control of process parameters

The effect of MAM's process parameters on the quality of product parts has been extensively studied. In order to establish the basis of process control, the process parameters, signal characteristics and build quality are correlated and classified according to the ability to be measured or controlled [163,164]. Taking SLM process as an example, the quality of build is mainly related to powder properties, machine properties, chamber environment, process parameters and post-processing technics. The controllable process parameters are related to laser power, scanning speed, hatch distance, powder thickness, through which the SLM process can be optimized and the build quality can be controlled. These parameters are included in the laser energy density $\boldsymbol{E}$, defined as [4],

$$E = \frac{P}{v \times h \times d} \tag{11}$$

where P laser power, v laser scanning speed, h is the hatch distance, d is the layer thickness. These influencing parameters that determine the laser energy density directly affect the performance of melting build, which also provides the possibility for feedback control through process parameter monitoring.

The MAM control system is mainly composed of laser power control, powder spreading control, powder preheating control and temperature control. The control of laser power is critical for improving the quality of build with complex geometry. As can be seen from Eq. (4), the laser power essentially determines the energy density when the process parameters are preset. When the laser power is too low, it will result in a small melt pool and lack of fusion, and if the laser power is too high, it may result in keyhole and material evaporation [2,4,21]. These become more significant when the scanning mode changes suddenly, e.g., at laser turnarounds for a multi-track build, the returning end of the track was heated repeatedly and lead to keyhole formation and material evaporation [4,32,33]. As a result, to eliminate overmelting or keyhole-induced porosity at track ends, laser power control is necessary to achieve a high quality build.

The powder spreading control system is one of the core components of the whole PBF technology. The thickness, surface

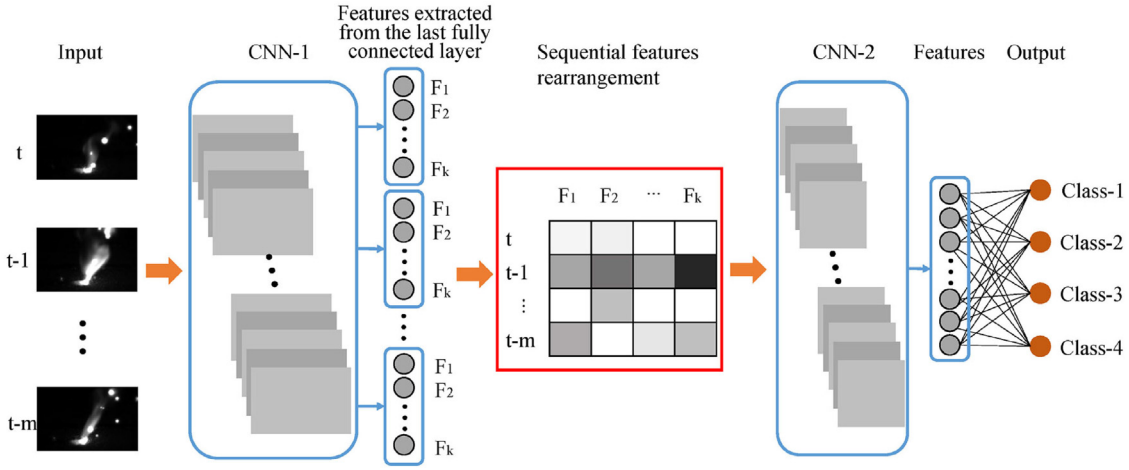

Fig. 12. The architecture of the hybrid CNNs model [157].

smoothness, powder spreading density and accuracy of the powder spreading all have an impact on the processing results, and are also the main factors affecting the final build accuracy. According to the bulk density and the surface quality parameters of the powder, the experiments on different powder spreading control systems were carried out and studied [165]. The highest density and the best surface quality could be obtained by using the 22 mm diameter reverse roller system. Preheating is an extremely important stage in the building process, and its accuracy is vital to the build time, accuracy and strength of the build. The preheating temperature control of EBM process was attempted with the thermal camera of NIR (near infrared) two lenses [166], with the temperature range 600–3000°C. It could effectively measure the different temperature ranges (low, medium) of each stage (preheating, contour build) in the process control. In the SLS process, when there was no preheating control system between adjacent layers, the temperature of the upper layer was high and the temperature of the lower layer reduced rapidly [167], which would eventually lead to warping. Buchbinder et al. [168] investigated the effects of preheating during SLM of aluminum components and determined an appropriate preheating temperature to eliminate distortions. A significant reduction of distortion could be observed at a preheating temperature of 150 °C. Additionally, a proper preheating avoided the stress-related cracks in the build. The preheating control system has strict requirements for temperature stability, and the bed temperature must be kept consistently in a certain range.

Due to the local characteristics of laser beam heating, it causes uneven temperature field and large temperature gradient, which will lead to balling, warping and cracking of the build [4]. It is very necessary to study the control of temperature field. Dai et al. [170] proposed a finite element analysis method to investigate the influence of laser scanning mode on residual stress and deformation. The study showed that if there was a layer of deformation, changing the laser scanning mode could minimize the influence of it. The study also found that, if the scanning path was scanned for a long distance along the axis, saddle distortion might occur.

In the DED process, the mechanical properties of the deposited materials depend on the solidification microstructure, which is mostly determined by the melt pool temperature and cooling rate. As a result, it is crucial to monitor and control these two signals to obtain high-quality products [171]. Farshidianfar et al. [169] developed a feedback control method for real-time control of deposition microstructure in MAM process (Fig. 13). An infrared imaging system was designed to monitor the surface temperature and a feedback PID controller was developed to control the cooling rate by establishing the relation of cooling rate, traveling speed and microstructure. A consistently controlled microstructure, i.e., grain size, cellular dendrite growth, volumetric percentage of the columnar and cellular regions, could finally be reached in real time. These approaches are helpful to realize the flexible build preparation and the control of the build microstructure. However, they are still constrained by the limitation of spatial resolution and observation area of the monitoring system, as well as the real-time performance of the control method.

5.2. The control strategies

The majority of the existing literatures on process control of MAM were based on empirical models, while physics-based models are less studied. The melt pool is most studied for the process control due to its importance in determining the building quality. Song et al. [172,173] designed an online control system for DED process to control deposition height and melt pool temperature. In the melt pool temperature control, a state space model describing the dynamic relationship between laser power and molten pool temperature was obtained through system identification. Based on the state space model, a generalized model predictive control (MPC) algorithm was designed. The experimental results showed that the temperature control system could effectively relieve the shrinkage of the deposition layer, and greatly improved the build quality. Bi et al. [174] applied PID controller for the melt pool temperature control. It studied the effects of scanning rate, laser power and powder feeding rate on the temperature of melt pool. There were significant errors found in detecting the temperature of the melt pool in the lateral direction. Hu et al. [175] used the infrared CCD imaging system of coaxial detection to monitor the melt pool and its surrounding area. The width of the melt pool was controlled by adjusting the laser power. In the case of lower laser power, there was a linear relationship between the size and the average temperature of the melt pool. To control the size of molten pool is essentially to control the temperature of melt pool, which is more eminent for materials with high thermal conductivity. More similar study was reported for melt pool temperature control in DED process [176].

For online process control, the simplified control model is more popular than numerical models (i.e., finite element method (FEM)) due to the computational efficiency. Tang and landers [177] proposed a height controller for DED process, which consist of two differential and three algebraic equations derived from mass, momentum and energy balance. The height controller had

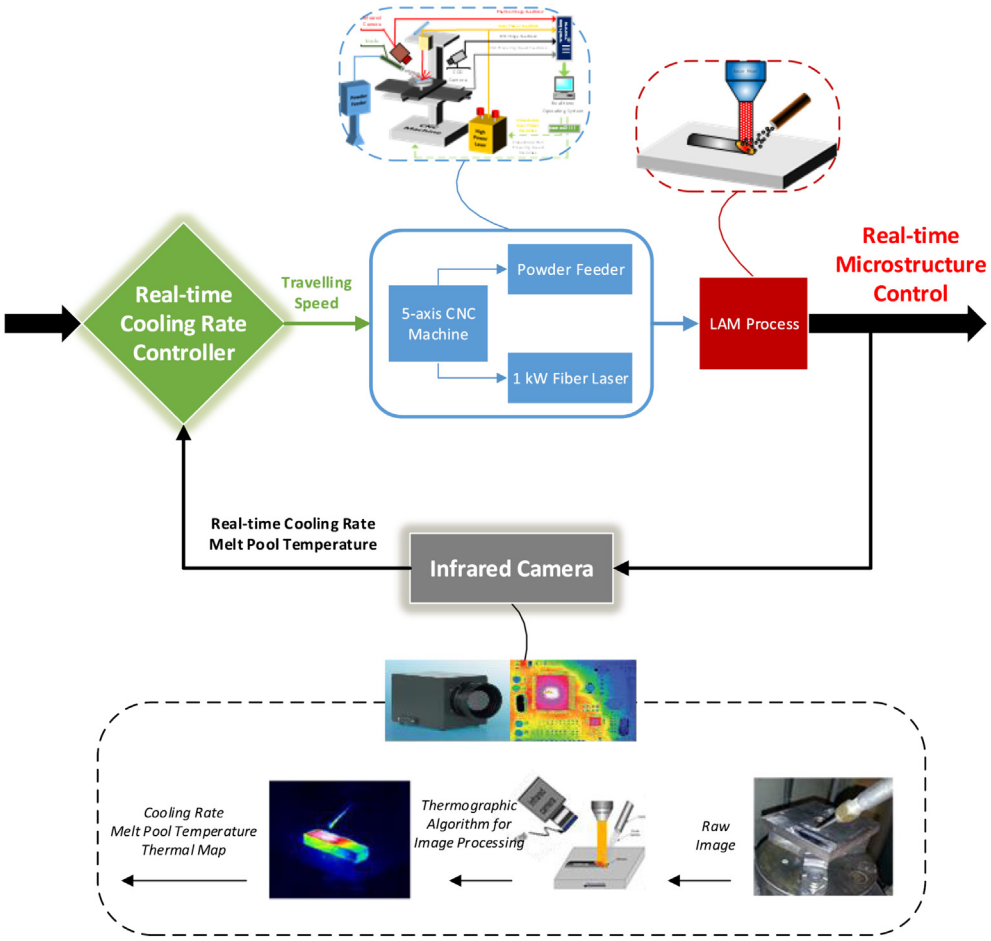

Fig. 13. Block diagram of real-time micro structure controller [169].

three main parts: measurement (height and temperature), system identification and powder flow rate reference generation. The iterative learning control method was then used to generate the powder flow rate reference distribution based on the estimated model, which would generate the specified layer height reference. Fig. 14 showed the height distribution experiment using layer and layer height control. It could be seen that the increment of layer height was more uniform when using layer and layer height control than when using constant powder flow rate experiment. The final orbit height was very close to the reference orbit height with an average error of 1.00%. The average error was about 24.80% when a constant powder flow rate was used.

Steuben et al. [178] developed an enriched analytic solution method for the AM feedback control, which included the handling of strong nonlinear variations in material properties, behavior of heat sources near boundaries, and coupled mass accretion problems. The results were shown equivalent to numerical methods but with much less computational cost. Zheng et al. [179] proposed a PDE-based approach for the distributed temperature control in MAM process. It modeled the laser velocity and power to regulate the temperature in the moving laser frame to achieve the desired performance in terms of the cooling rate and melt pool width. Li et al. [180] developed a lumped-parameter model of melt-pool geometry for DED process control of multi-track, multi-layer builds. Based on this model, a nonlinear feed-forward controller was derived to control laser power to build an L-shape Ti-6AL-4V part for a given height. The study was furthered for SLM process [181], where both feedforward and feedback controller were established to maintain the melt-pool geometry so as to reduce the lack-of-fusion and porosity.

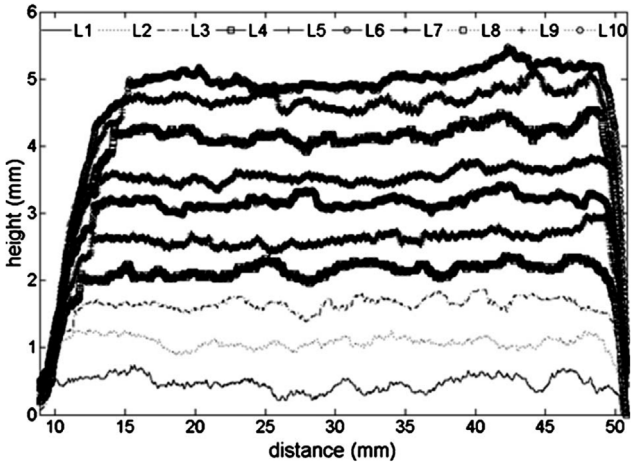

Fig. 14. Height curve of the experiments using layer–layer height control [177].

Due to the complex interactions and the inherent multi-input–multi-output (MIMO) process characteristics, simultaneous monitoring and regulation of these factors are often required, which generally lead to elaborated models of nonlinear partial differential equations that described the complex multi-physics interactions. They are not analytically nor computationally efficient from control perspectives. In this sense, the ordinary differential equation based lumped parameter models were studied [172, 173,176,182]. Cao and Ayalew [183] developed an MIMO process

model to achieve desired geometrical and thermal properties, which was formulated as one of generating and tracking nominal reference profiles of layer height and melting pool temperature. This was accomplished via a nonlinear MPC with guaranteed nominal stability. Furthermore, a local ancillary feedback law was derived to provide robustness to bounded uncertainties.

At present, most of the control methods of melt pool temperature are based on the improved PID algorithm. This kind of control is simple in structure and easy to design, but in practice, the PID controller is hard to handle the multiple constraints in MAM system. In addition, to keep the melt pool temperature consistent, it is necessary to limit the variation rate of laser power. However, the noise and disturbance of the environment will lead to strong instability of the system, which will result in the abnormal processing. At the same time, the MAM process is a complex physical-metallurgical process and often difficult to establish an accurate physical model for control. When the model is complex the computational cost is usually high, which makes it cannot get back the results in a single control cycle and hard to implement online.

6. Conclusions and futures studies

This study investigated the state-of-the-art MAM process monitoring methods, in which the important aspects such as process measurement, signal acquisition, feature extraction, classification and control approaches are summarized and reviewed, and their corresponding advantages and disadvantages are discussed. As shown in the literatures, the data-oriented process monitoring approaches provide a reliable basis for improving the build quality and process stability, and lay the technical foundation of additive manufacturing automation and control. Although great progress has been made in the research, there are still a lot of challenging problems, both from theory to applications, to be further studied.

(1) Physical model based process monitoring. In MAM processes, the quantitative description of physical models, which include material science, thermo-fluid phenomenon and process equipment interactions, is still in the initial stage. The current MAM monitoring methods are either offline or pure data-driven (machine learning, statistical analysis), and their role is usually simplified as the production process anomaly detection. In the absence of a physical model, the adaption and prediction capabilities of the data-driven models are limited. In order to realize closed-loop control of MAM process, it is necessary to combine physical model with data-driven models in the future study. This may be implemented by hybrid combining the physical model and ML based models for the fusion of the decision, or by developing the physical-guided loss function for the ML model to realize the cyber–physical monitoring system (or digital twin).

(2) From monitoring the surface state to the internal defect and microstructure. In the current monitoring approaches, the radiation intensity of the melt pool is often measured to realize the macro morphology monitoring of the builds. With the advancement of measurement technology, the online monitoring of internal defects has become possible, i.e. the grain structure, which will lay a foundation for real-time microstructure control and incipient defect repair.

(3) Multi-information fusion. Future studies should utilize various monitoring methods for different processing stages according to different types of measurements. This will overcome for the limitations of single source and avoid the decision uncertainty. By the multi-information fusion, the monitoring system will eventually realize the comprehensive evaluation of multi-sensor measurements of the process, and improve the accuracy and reliability of the monitoring system.

(4) Special sensing method. Because of its special material processing mechanics of MAM processes, conventional sensors that are widely applied in manufacturing process monitoring may not be the best choice. For example, accelerometers, force sensors and acoustic emission sensors can be used to detect the machining process, but they play a limited role in MAM. Although sensors based on laser, acoustic, thermo-optical, infrared and other technologies have been widely used, the special sensing technology for MAM quality detection still needs further investigation.

(5) Active online monitoring. The current MAM process monitoring setups are mostly based on optical imaging, and it is limited by working environment such as lighting conditions, metal evaporation, and high temperature conditions. Active monitoring technology, i.e., the optical low-coherent interferometry applied to SLM process and the electron optical imaging applied to EBM process, can reduce the requirements of working environment by actively emitting measuring beam. These active monitoring approaches could improve the sensitivity, anti-interference ability and adaptability to working environment of the measuring system. It would be a valuable and promising direction in the future research.

Declaration of competing interest

The authors declare that they have no known competing financial interests or personal relationships that could have appeared to influence the work reported in this paper.

Acknowledgment

This project is supported by the National Natural Science Foundation of China (Grant No. 51805384, No. 51875379).

References

[1] ASTM. Standard Terminology for Additive Manufacturing, StandArd No. ASTM 52900-15. West Conshohocken, PA: ASTM International; 2015.
[2] Bian L, Shamsaei N, Usher JM. Laser-Based Additive Manufacturing of Metal Parts: Modeling, Optimization, and Control of Mechanical Properties. CRC Press; 2018.
[3] Gu D, Meiners W, Wissenbach K, Poprawe R. Laser additive manufacturing of metallic components: materials, processes and mechanisms. Int Mater Rev 2012;57:133–64.
[4] Debroy T, Wei H, Zuback J, Mukherjee T, Zhang W. Additive manufacturing of metallic components-process, structure and properties. Prog Mater Sci 2018;92:112–224.
[5] Mumtaz K, Hopkinson N. Top surface and side roughness of inconel 625 parts processed using selective laser melting. Rapid Prototyping J 2009;15(2):96–103.
[6] Li R, Liu J, Shi Y, Wang L, Jiang W. Balling behaviour of stainless steel and nickel powder during selective laser melting process. Int J Adv Manuf Tech 2012;59(9):1025–35.
[7] Zhang B, Li Y, Bai Q. Defect formation mechanisms in selective laser melting: a review. Chin J Mech Eng 2017;30:515–27.
[8] Gong H, Rafi K, Gu H, Starr T, Stucker B. Analysis of defect generation in Ti–6Al–4V parts made using powder bed fusion additive manufacturing processes. Addit Manuf 2014;1–4:87–98.
[9] Phuc LT, Seita M. A high-resolution and large field-of-view scanner for in-line characterization of powder bed defects during additive manufacturing. Mater Des 2019;164:107562.
[10] Zur Jacobsmuhlen J, Kleszczynski S, Witt G, Merhof D. Detection of elevated regions in surface images from laser beam melting processes. In: IECON 2015-41st Annual Conference of the IEEE Industrial Electronics Society. 2015, 15753163.
[11] Weingarten C, Buchbinder D, Pirch N, Meiners W, Wissenbach K, Poprawe R. Formation and reduction of hydrogen porosity during selective laser melting of AlSi10Mg. J Mater Process Tech 2015;221:112–20.
[12] Tang M, Pistorius PC, Beuth JL. Prediction of lack-of-fusion porosity for powder bed fusion. Addit Manuf 2017;14:39–48.
[13] DePond PJ, Guss G, Ly S, Calta NP, Deane D, Matthews MJ, Khairallah S. In situ measurements of layer roughness during laser powder bed fusion additive manufacturing using low coherence scanning interferometry. Mater Des 2018;154:347–59.

[14] Leach R, Bourell D, Carmignato S, Dewulf W. Geometrical metrology for metal additive manufacturing. CIRP Ann-Manuf Techn 2019;68(2):677–700.
[15] Mani M, Lane B, Donmez A, Feng S, Moylan S, Fesperman R. Measurement science needs for real-time control of additive manufacturing powder bed fusion processes. In: StandArd No. NISTIR 8036. Gaithersburg, MD: National Institute of Standards and Technology; 2015.
[16] Mani M, Lane BM, Donmez MA, Feng SC, Moylan SP. A review on measurement science needs for real-time control of additive manufacturing metal powder bed fusion processes. Int J Prod Res 2017;55(5):1400–18.
[17] Purtonen T, Kalliosaari A, Salminen A. Monitoring and adaptive control of laser processes. Physics Procedia 2014;56:1218–31.
[18] Khairallah SA, Anderson AT, Rubenchik A, King WE. Laser powder-bed fusion additive manufacturing: physics of complex melt flow and formation mechanisms of pores, spatter, and denudation zones. Acta Mater 2016;108:36–45.
[19] Bidare P, Bitharas I, Ward RM, Attalla MM, Moore AJ. Fluid and particle dynamics in laser powder bed fusion. Acta Mater 2018;142:107–20.
[20] Spears TG, Gold SA. In-process sensing in selective laser melting (SLM) additive manufacturing. Integr Mater Manuf I 2016;5(1):16–40.
[21] Clijsters S, Craeghs T, Buls S, Kempen K, Kruth JP. In situ quality control of the selective laser melting process using a high-speed, real-time melt pool monitoring system. Int J Adv Manuf Technol 2014;75(5–8):1089–101.
[22] Charalampous P, Kostavelis I, Tzovaras D. Non-destructive quality control methods in additive manufacturing: a survey. Rapid Prototyping J 2020;26(4):777–90.
[23] Everton SK, Hirsch M, Stravroulakis P, Leach RK, Clare AT. Review of in-situ process monitoring and in-situ metrology for metal additive manufacturing. Mater Des 2016;95:431–45.
[24] Chua ZY, Ahn IH, Moon SK. Process monitoring and inspection systems in metal additive manufacturing: status and applications. Int J Precis Eng Manuf Green Technol 2017;4(2):235–45.
[25] Malekipour E, El-Mounayri H. Common defects and contributing parameters in powder bed fusion am process and their classification for online monitoring and control: a review. Int J Adv Manuf Technol 2018;95(1–4):527–50.
[26] Grasso M, Colosimo BM. Process defects and in situ monitoring methods in metal powder bed fusion: a review. Meas Sci Technol 2017;28(4):044005.
[27] Reutzel EW, Nassar AR. A survey of sensing and control systems for machine and process monitoring of directed-energy, metal based additive manufacturing. Rapid Prototyping J 2015;21(2):159–67.
[28] Tapia G, Elwany A. A review on process monitoring and control in metal-based additive manufacturing. J Manuf Sci E-T ASME 2014;136(6):060801.
[29] SLM Solutions: https://slm-solutions.us/product/process-monitoring.
[30] EOS Monitoring systems: https://www.eos.info/software/monitoring-software.
[31] Lott P, Schleifenbaum H, Meiners W, Wissenbach K, Hinke C, Bültmann J. Design of an optical system for the in situ process monitoring of selective laser melting (SLM). Physics Procedia 2011;12:683–90.
[32] Arisoy YM, Criales LE, Özel T, Lane B, Moylan S, Donmez A. Influence of scan strategy and process parameters on microstructure and its optimization in additively manufactured nickel alloy 625 via laser powder bed fusion. Int J Adv Manuf Tech 2017;90(5–8):1393–417.
[33] Shamsaei N, Yadollahi A, Bian L, Thompson SM. An overview of direct laser deposition for additive manufacturing part ii: mechanical behavior, process parameter optimization and control. Addit Manuf 2015;8:12–35.
[34] Dilip JJS, Zhang S, Teng C, Zeng K, Robinson C, Pal D, Stucker B. Influence of processing parameters on the evolution of melt pool, porosity, and microstructures in ti-6al-4v alloy parts fabricated by selective laser melting. Prog Addit Manuf 2017;2(3):157–67.
[35] Whip B, Sheridan L, Gockel J. The effect of primary processing parameters on surface roughness in laser powder bed additive manufacturing. Int J Adv Manuf Tech 2019;103:4411–22.
[36] Schmidt M, Merklein M, Bourell D, Dimitrov D, Hausotte T, Wegener K, Overmeyer L, Vollertsen F, Levy GN. Laser based additive manufacturing in industry and academia. CIRP Ann-Manuf Techn 2017;66:561–83.
[37] Baturynska I, Semeniuta O, Martinsen K. Optimization of process parameters for powder bed fusion additive manufacturing by combination of machine learning and finite element method: a conceptual framework. Procedia CIRP 2018;67(1):227–32.
[38] Berumen S, Bechmann F, Lindner S, Kruth JP, Craeghs T. Quality control of laser- and powder bed-based additive manufacturing (AM) technologies. Physics Procedia 2010;5:617–22.
[39] Craeghs T, Bechmann F, Berumen S, Kruth JP. Feedback control of layerwise laser melting using optical sensors. Physics Procedia 2010;5:505–14.
[40] Craeghs T, Clijsters S, Kruth JP, Bechmann F, Ebert MC. Detection of process failures in layerwise laser melting with optical process monitoring. Physics Procedia 2012;39:753–9.
[41] Clijsters S, Craeghs T, Buls S. In situ quality control of the selective laser melting process using a high-speed, real-time melt pool monitoring system. Int J Adv Manuf Tech 2014;75:1089–101.
[42] Lott P, Schleifenbaum H, Meiners W. Design of an optical system for the in situ process monitoring of selective laser melting (SLM). Physics Procedia 2011;12:683–90.
[43] Yadroitsev I, Krakhmalev P, Yadroitsava I. Selective laser melting of ti6al4v alloy for biomedical applications: Temperature monitoring and microstructural evolution. J Alloy Compd 2014;583:404–9.
[44] Wegner A, Witt G. Process monitoring in laser sintering using thermal imaging. In: Solid Free Fabr Symp Proc. 2011, p. 405–14.
[45] Chivel Y, Smurov I. On-line temperature monitoring in selective laser sintering/melting. Physics Procedia 2010;5:515–21.
[46] Chivel Y. Ablation phenomena and instabilities under laser melting of powder layers. In: 8th International Conference on Photonic Technologies LANE. 2014, p. 1–7.
[47] Islam M, Purtonen T, Piili H, Salminen A, Nyrhilä O. Temperature profile and imaging analysis of laser additive manufacturing of stainless steel. Physics Procedia 2013;41:835–42.
[48] Furumoto T, Ueda T, Alkahari MR, Hosokawa A. Investigation of laser consolidation process for metal powder by two-color pyrometer and high-speed video camera. CIRP Ann-Manuf Techn 2013;62:223–6.
[49] Kleszczynski S, Joschka ZJ, Sehrt JT, Witt G. Error detection in laser beam melting systems by high resolution imaging. In: Solid Free Fabr Symp Proc. 2012, p. 975–87.
[50] Pavlov M, Doubenskaia M, Smurov I. Pyrometric analysis of thermal processes in SLM technology. Physics Procedia 2010;5:523–31.
[51] Krauss H, Eschey C, Zaeh M. Thermography for monitoring the selective laser melting process. In: Solid Free Fabr Symp Proc. 2012, p. 999–1014.
[52] Dadbakhsh S, Hao L, Sewell N. Effect of selective laser melting layout on the quality of stainless steel parts. Rapid Prototyping J 2012;18:241–9.
[53] Kanko JA, Sibley AP, Fraser JM. In situ morphology-based defect detection of selective laser melting through inline coherent imaging. J Mater Process Tech 2016;231:488–500.
[54] Liu Y, Yang Y, Mai S, Wang D, Song C. Investigation into spatter behavior during selective laser melting of AISI 316L stainless steel powder. Mater Des 2015;87:797–806.
[55] Cheng D, Zhu H, Ke L. Investigation of plasma spectra during selective laser micro sintering Cu-based metal powder. Rapid Prototyping J 2013;19:373–82.
[56] Lane B, Moylan S, Whitenton EP, Ma L. Thermographic measurements of the commercial laser powder bed fusion process at NIST. In: Solid Free Fabr Symp Proc. 2015, p. 575–91.
[57] Lane B, Whitenton E, Moylan S. Multiple sensor detection of process phenomena in laser powder bed fusion, In: Proceedings of SPIE; 2016, p. 9861041–9861049.
[58] Matilainen VP, Piili H, Salminen A, Nyrhilä O. Preliminary investigation of keyhole phenomena during single layer fabrication in laser additive manufacturing of stainless steel. Physics Procedia 2015;78:377–87.
[59] Rieder H, Dillhöfer A, Spies M, Bamberg J, Hess T. Ultrasonic online monitoring of additive manufacturing processes based on selective laser melting. In: AIP Conference Proceedings. 2015, p. 184–91.
[60] Ye D, Hong GS, Zhang Y, Zhu K, Fuh JYH. Defect detection in selective laser melting technology by acoustic signals with deep belief networks. Int J Adv Manuf Tech 2018;96(5):2791–801.
[61] Smith RJ, Hirsch M, Patel R, Li W, Clare AT, Sharples SD. Spatially resolved acoustic spectroscopy for selective laser melting. J Mater Process Tech 2016;236:93–102.
[62] Hippert D, Jhabvala J, Boillat E, Santi G, Bleuler H. Development of an eddy current testing method as process control for additive manufacturing of metallic components. In: Proceedings of the 14th IFToMM World Congress; 2015: p. 10–14.
[63] Belle LV, Vansteenkiste G, Boyer JC. Investigation of residual stresses induced during the selective laser melting process. Key Eng Mater 2013;554:1828–34.
[64] Zenzinger G, Bamberg J, Ladewig A, Hess T, Henkel B, Satzger W. Process monitoring of additive manufacturing by using optical tomography. In: AIP Conference Proceedings 1650; 2015: p. 164–70.
[65] Andani MT, Dehghani R, Karamooz MR, Mirzaeifar R, Ni J. Spatter formation in selective laser melting process using multi-laser technology. Mater Des 2017;131:460–9.
[66] Khosroshahi ME, Anooshehpour F, Hadavi M, Mahmoodi M. In situ monitoring the pulse CO2 laser interaction with 316-l stainless steel using acoustical signals and plasma analysis. Appl Surf Sci 2010;256(24):7421–7.
[67] Koester LW, Bond LJ, Taheri H, Collins PC. Nondestructive evaluation of additively manufactured metallic parts. In: Additive Manufacturing for the Aerospace Industry. CRC press; 2019, p. 401–17.

[68] Grasso M, Gallina F, Colosimo BM. Data fusion methods for statistical process monitoring and quality characterization in metal additive manufacturing. Procedia CIRP 2018;75:103–7.
[69] Mallat SG. Wavelet Tour of Signal Processing. second ed.. Academic Press; 1998.
[70] Barrett C, Carradero C, Harris E, McKnight J, Walker J, MacDonald E, Conner B. Low cost, high speed stereovision for spatter tracking in laser powder bed fusion. In: Solid Free Fabr Symp Proc. 2018, p. 2122–34.
[71] Mazzoleni L, Demir AG, Caprio L, Pacher M, Previtali B. Real-time observation of melt pool in selective laser melting: spatial, temporal and wavelength resolution criteria. IEEE T Instrum Meas 2019;69(4):1179–90.
[72] Zhao C, Fezzaa K, Cunningham RW, Wen H, DeCarlo F, Chen L, Rollett AD, Sun T. Real-time monitoring of laser powder bed fusion process using high-speed X-ray imaging and diffraction. Sci Rep 2017;7(1):3602.
[73] Cheng B, Lydon J, Cooper K, Cole V, Northrop P, Chou K. Melt pool dimension measurement in selective laser melting using thermal imaging. In: Solid Free Fabr Symp Proc. 2017, p. 1252–63.
[74] Islam M, Purtonen T, Piili H, Salminen A, Nyrhilä O. Temperature profile and imaging analysis of laser additive manufacturing of stainless steel. Phys. Procedia 2013;41:835–42.
[75] Krauss H, Eschey C, Zaeh MF. Thermography for monitoring the selective laser melting process. In: Solid Free Fabr Symp Proc. 2012, p. 999–1014.
[76] Doubenskaia M, Grigoriev S, Zhirnov I, Smurov I. Parametric analysis of SLM using comprehensive optical monitoring. Rapid Prototyping J 2016;22(1):40–50.
[77] Smith RJ, Hirsch M, Patel R, Li W, Clare AT, Sharples SD. Spatially resolved acoustic spectroscopy for selective laser melting. J. Mater. Process. Tech. 2016;236:93–102.
[78] Gaja H, Liou F. Defects monitoring of laser metal deposition using acoustic emission sensor. Int J Adv Manuf Technol 2017;90(1–4):561–74.
[79] Rieder H, Dillhöfer A, Spies M, Bamberg J, Hess T. Ultrasonic online monitoring of additive manufacturing processes based on selective laser melting. In: AIP Conference Proceedings. 2015, p. 84–91.
[80] Taheri H, Koester LW, Bigelow TA, Faierson EJ, Bond LJ. In-situ additive manufacturing process monitoring with an acoustic technique: clustering performance evaluation using K-means algorithm. J Manuf Sci E-T ASME 2019;141(4):041011.
[81] Strantza M, Hemelrijck DV, Guillaume P, Aggelis DG. Acoustic emission monitoring of crack propagation in additively manufactured and conventional titanium components. Mech Res Commun 2017;84:8–13.
[82] Koester LW, Taheri H, Bigelow TA, Bond LJ, Faierson EJ. In-situ acoustic signature monitoring in additive manufacturing processes. AIP Conf Proc 2018;1949:020006.
[83] Ye D, Hong GS, Zhang Y, Zhu K, Fuh JYH. Defect detection in selective laser melting technology by acoustic signals with deep belief networks. Int J Adv Manuf Tech 2018;593(1):170.
[84] Eschner N, Weiser L, Häfner B, Lanza G. Development of an acoustic process monitoring system for selective laser melting (SLM). In: Solid Free Fabr Symp Proc. 2018, p. 2097–117.
[85] Kanko JA, Sibley AP, Fraser JM. In situ morphology-based defect detection of selective laser melting through inline coherent imaging. J Mater Process Tech 2016;231:488–500.
[86] Tang J, Zuo D, Jiu Z, Cheng Z. Spectral property investigation of air plasma generated by pulsed CO2 laser. IEEE T Plasma Sci 2011;39(4):1114–9.
[87] zur Jacobsmühlen J, Kleszczynski S, Witt G, Merhof D. Compound quality assessment in laser beam melting processes using layer images. In: IEEE International Instrumentation and Measurement Technology Conference (I2MTC), 2017. 2017, p. 1–6.
[88] Stutzman CB, Nassar AR, Reutzel EW. Multi-sensor investigations of optical emissions and their relations to directed energy deposition processes and quality. Addit Manuf 2018;21:333–9.
[89] Lane B, Whitenton E, Moylan S. Multiple Sensor Detection of Process Phenomena in Laser Powder Bed Fusion. International Society for Optics and Photonics; 2016, p. 9861041–9.
[90] Montazeri M, Rao P. Sensor-based build condition monitoring in laser powder bed fusion additive manufacturing process using a spectral graph theoretic approach. J Manuf Sci E-T ASME 2018;140(9):091002.
[91] Scime L, Beuth J. A multi-scale convolutional neural network for autonomous anomaly detection and classification in a laser powder bed fusion additive manufacturing process. Addit Manuf 2018;24:273–86.
[92] Kouprianoff D, Luwes N, Yadroitsava I, Yadroitsev I. Acoustic emission technique for online detection of fusion defects for single tracks during metal laser powder bed fusion. In: Solid Free Fabr Symp Proc. 2018, p. 2087–96.
[93] Shevchik SA, Masinelli G, Kene C, Leinenbach C, Wasmer K. Deep learning for in situ and real-time quality monitoring in additive manufacturing using acoustic emission. IEEE T Ind Inform 2019;15(9):5194–203.
[94] Shevchik SA, Le QT, Meylan B, Wasmer K. Acoustic emission for in situ monitoring of laser processing. In: 33rd European Conference on Acoustic Emission Testing (EWGAE 2018). 2018, p. 1–10.
[95] Hirsch M, Patel R, Li W, Guan G, Leach RK, Sharples SD, Clare AT. Assessing the capability of in-situ nondestructive analysis during layer based additive manufacture. Addit Manuf 2017;13:135–42.
[96] Lu QY, Wong CH. Additive manufacturing process monitoring and control by non-destructive testing techniques: challenges and in-process monitoring. Virtual Phys Prototy 2018;13(2):39–48.
[97] Wasmer K, Le-Quang T, Meylan B, Shevchik SA. In situ quality monitoring in AM using acoustic emission: A reinforcement learning approach. J Mater Eng Perform 2019;28(2):666–72.
[98] Sibillano T, Ancona A, Rizzi D, Lupo V, Tricarico L, Lugarà PM. Plasma plume oscillations monitoring during laser welding of stainless steel by discrete wavelet transform application. Sensors 2010;10(4):3549–61.
[99] Vakili-Farahani F, Lungershausen J, Wasmer K. Wavelet analysis of light emission signals in laser beam welding. J Laser Appl 2017;29(2):022424.
[100] Fisher KA, Candy JV, Guss G, Mathews JM. Evaluating Acoustic Emission Signals As an in Situ Process Monitoring Technique for Selective Laser Melting (SLM) (No. LLNL-TR-706659). Lawrence Livermore National Laboratory (LLNL); 2016.
[101] Salloum M, Johnson KL, Bishop JE, Aytac JM, Dagel D, van Bloemen Waanders BG. Adaptive wavelet compression of large additive manufacturing experimental and simulation datasets. Comput Mech 2019;63:491–510.
[102] Coifman RR, Wickerhauser MV. Entropy- based algorithms for best basis selection. IEEE Trans Inform Theom 1992;38:713–8.
[103] Craeghs T, Clijsters S, Yasa E, Bechmann F, Berumen S, Kruth JP. Determination of geometrical factors in layerwise laser melting using optical process monitoring. Opt Lasers Eng 2011;49(12):1440–6.
[104] Aminzadeh M. A Machine Vision System for in-Situ Quality Inspection in Metal Powder-Bed Additive Manufacturing (Ph.D. thesis), Georgia Institute of Technology; 2016.
[105] Aminzadeh M, Kurfess TR. Kurfess TR online quality inspection using Bayesian classification in powder-bed additive manufacturing from high-resolution visual camera images. J Intell Manuf 2018;30:2505–23.
[106] Sonka M, Hlavac V, Boyle R. Image processing, analysis, and machine vision. In: Cengage Learning. 2014.
[107] Nixon MS, Aguado AS. Feature Extraction & Image Processing for Computer Vision. Academic Press; 2012.
[108] Cheng HD, Jiang XH, Sun Y, Wang J. Color image segmentation: advances and prospects. Pattern Recognit 2001;34(12):2259–81.
[109] Ridler TW, Calvard S. Picture thresholding using an iterative selection method. IEEE Trans Syst Man Cybern 1978;8:630–2.
[110] Otsu N. A threshold selection method from gray-level histograms. IEEE Trans Syst Man Cybern 1979;9(1):62–6.
[111] Li CH, Tam PKS. An iterative algorithm for minimum cross entropy thresholding. Pattern Recognit Lett 1998;18(8):771–6.
[112] Huang LK, Wang MJJ. Image thresholding by minimizing the measure of fuzziness. Pattern Recognit 1995;28(1):41–51.
[113] Grasso M, Demir AG, Previtali B, Colosimo BM. In situ monitoring of selective laser melting of zinc powder via infrared imaging of the process plume. Robot Cim-Int Manuf 2018;49:229–39.
[114] Lowe DG. Distinctive image features from scale-invariant keypoints. Int J Comput Vision 2004;60(2):91–110.
[115] Dalal N, Triggs B. Histograms of oriented gradients for human detection. In: IEEE Conference Computer Vision and Pattern Recognition. 2005, p. 886–93.
[116] Mikolajczyk K, Schmid C. A performance evaluation of local descriptors. IEEE T Pattern Anal 2005;27(10):1615–30.
[117] Abdelrahman M, Reutzel EW, Nassar AR, Starr TL. Flaw detection in powder bed fusion using optical imaging. Addit Manuf 2017;15:1–11.
[118] Li Z, Liu X, Wen S, He P, Zhong K, Wei Q, Liu S. In situ 3d monitoring of geometric signatures in the powder-bed-fusion additive manufacturing process via vision sensing methods. Sensors 2018;18(4):1180.
[119] Foster BK, Reutzel EW, Nassar AR, Hall BT, Brown SW, Dickman CJ. Optical, layerwise monitoring of powder bed fusion. In: Solid Free Fabr Symp Proc. 2015, p. 295–307.
[120] Zhang B, Ziegert J, Farahi F, Davies A. In situ surface topography of laser powder bed fusion using fringe projection. Addit Manuf 2016;12:100–7.
[121] Jacobsmühlen J, Achterhold J, Kleszczynski S, Witt G, Merhof D. In situ measurement of part geometries in layer images from laser beam melting processes. Progress in Addit Manuf 2019;4(2):155–65.
[122] Gobert C, Reutzel EW, Petrich J, Nassar AR, Phoha S. Application of supervised machine learning for defect detection during metallic powder bed fusion additive manufacturing using high resolution imaging. Addit Manuf 2018;21:517–28.
[123] Scime L, Beuth J. Anomaly detection and classification in a laser powder bed additive manufacturing process using a trained computer vision algorithm. Addit Manuf 2018;19:114–26.
[124] Caltanissetta F, Grasso M, Petrò S, Colosimo BM. Characterization of in-situ measurements based on layerwise imaging in laser powder bed fusion. Addit Manuf 2018;24:183–99.

[125] Imani F, Gaikwad A, Montazeri M, Rao P, Yang H. Process mapping and in-process monitoring of porosity in laser powder bed fusion using layerwise optical imaging. J Manuf Sci E-T ASME 2018;140(10):101009-14.
[126] Yao B, Imani F, Sakpal AS, Reutzel EW, Yang H. Multifractal analysis of image profiles for the characterization and detection of defects in additive manufacturing. J Manuf Sci E-T ASME 2018;140(3):031014.
[127] Bishop CM. Pattern Recognition and Machine Learning. Springer; 2006.
[128] Bengio Y, Goodfellow I, Courville A. Deep Learning. MIT presss; 2016.
[129] Qi X, Chen G, Li Y, Cheng X, Li C. Applying neural-network-based machine learning to additive manufacturing: current applications, challenges, and future perspectives. Engineering 2019;5:721–9.
[130] Shen X, Yao J, Wang Y, Yang J. Density prediction of selective laser sintering parts based on artificial neural network. In: Advances in Neural Networks-ISNN. 2004, p. 153–65.
[131] Wang RJ, Li XH, Wu QD, Wang LL. Optimizing process parameters for selective laser sintering based on neural network and genetic algorithm. Int J Adv Manuf Tech 2009;42:1035–42.
[132] Negi S, Sharma RK. Study on shrinkage behaviour of laser sintered PA 3200gf specimens using RSM and ANN. Rapid Prototyping J 2016;22(4):645–59.
[133] Kwon O, Kim HG, Ham MJ, Kim W, Kim GH, Cho JH, Kim NI, Kim K. A deep neural network for classification of melt-pool images in metal additive manufacturing. J Intell Manuf 2020;31:375–86.
[134] Marrey M, Malekipour E, El-Mounayri H, Faierson EJ. A framework for optimizing process parameters in powder bed fusion (PBF) process using artificial neural network (ANN). Procedia Manuf 2019;34:505–15.
[135] Eschner N, Weiser L, Häfner B, Lanza G. Development of an acoustic process monitoring system for selective laser melting (SLM). In: Solid Free Fabr Symp Proc. 2018, p. 2097–3017.
[136] Caiazzo F, Caggiano A. Laser direct metal deposition of 2024 al alloy: trace geometry prediction via machine learning. Materials 2018;11(3):444.
[137] Khanzadeh M, Chowdhury S, Tschopp MA, Doude HR, Marufuzzaman M, Bian L. In-situ monitoring of melt pool images for porosity prediction in directed energy deposition processes. IISE Transactions 2019;51(5):437–55.
[138] Jafari-Marandi R, Khanzadeh M, Tian W, Smith B, Bian L. From in-situ monitoring toward high-throughput process control: cost-driven decision-making framework for laser-based additive manufacturing. J Manuf Syst 2019;51:29–41.
[139] Cai CZ, Pei JF, Wen YF, Zhu XJ, Xiao TT. Density prediction of selective laser sintering parts based on support vector regression. Acta Phys Sin 2009;58:S1–S19.
[140] Zhang Y, Hong GS, Ye D, Zhu K, Fuh JY. Extraction and evaluation of melt pool, plume and spatter information for powder-bed fusion am process monitoring. Mater Des 2018;156:458–69.
[141] Scime L, Beuth J. Using machine learning to identify in-situ melt pool signatures indicative of flaw formation in a laser powder bed fusion additive manufacturing process. Addit Manuf 2019;25:151–65.
[142] Seifi SH, Tian W, Doude H, Tschopp MA, Bian L. Layer-wise modeling and anomaly detection for laser-based additive manufacturing. J Manuf Sci E-T ASME 2019;141(8):081013.
[143] Gaja H, Liou F. Defects classification of laser metal deposition using acoustic emission sensor. In: Solid Free Fabr Symp Proc. 2017, p. 1952–64.
[144] Khanzadeh M, Chowdhury S, Marufuzzaman M, Tschopp MA, Bian L. Porosity prediction: supervised-learning of thermal history for direct laser deposition. J Manuf Syst 2018;47:69–82.
[145] Grasso M, Laguzza V, Semeraro Q, Colosimo BM. In-process monitoring of selective laser melting: spatial detection of defects via image (k-means). J Manuf Sci E-T ASME 2016;139(5):051001–1–16.
[146] Repossini G, Laguzza V, Grasso M, Colosimo BM. On the use of spatter signature for in-situ monitoring of laser powder bed fusion. Addit Manuf 2017;16:35–48.
[147] Uhlmann E, Pontes RP, Laghmouchi A, Bergmann A. Intelligent pattern recognition of a SLM machine process and sensor data. Procedia CIRP 2017;62:464–9.
[148] Okaro IA, Jayasinghe S, Sutcliffe CJ, Black K, Paoletti P, Green PL. Automatic fault detection for laser powder-bed fusion using semi-supervised machine learning. Addit Manuf 2019;27:42–53.
[149] Mahmoudi M, Ezzat AA, Elwany A. Layer-wise anomaly detection in laser powder-bed fusion metal additive manufacturing. J Manuf Sci E-T ASME 2019;141(3):031002.
[150] Ozel T, Shaurya A, Altay A, Yang L. Process monitoring of meltpool and spatter for temporal-spatial modeling of laser powder bed fusion process. Procedia CIRP 2018;74:102–6.
[151] Tapia G, Khairallah SA, Matthews MJ, Elwany A. Gaussian process-based surrogate modeling framework for process planning in laser powder-bed fusion additive manufacturing of 316L stainless steel. Int J Adv Manuf Tech 2018;94:3591–603.
[152] Montazeri M, Rao P. In-process condition monitoring in laser powder bed fusion (LPBF). In: Solid Free Fabr Symp Proc. 2017, p. 1264–78.
[153] Shevchik SA, Kenel C, Leinenbach C, Wasmer K. Acoustic emission for in situ quality monitoring in additive manufacturing using spectral convolutional neural networks. Addit Manuf 2018;21:598–604.
[154] Caggiano A, Zhang J, Alfieri V, Caiazzo F, Gao R, Teti R. Machine learning-based image processing for on-line defect recognition in additive manufacturing. CIRP Ann-Manuf Techn 2019;68:451–4.
[155] Imani F, Chen R, Diewald E, Reutzel E, Yang H. Deep learning of variant geometry in layerwise imaging profiles for additive manufacturing quality control. J Manuf Sci E-T ASME 2019;141(11):111001.
[156] Zhang B, Jaiswal P, Rai R, Baggs G. Convolutional neural network-based inspection of metal additive manufacturing parts. Rapid Prototyping J 2019;25(3):530–40.
[157] Zhang Y, Hong GS, Ye D, Fuh JYH, Zhu K. Powder-bed fusion process monitoring by machine vision with hybrid convolutional neural networks. IEEE T Ind Inform 2020;16(9). 5769–5779.
[158] Yuan B, Guss GM, Wilson AC, Hau-Riege SP, DePond PJ, McMains S, Matthews MJ, Giera B. Machine learning-based monitoring of laser powder bed fusion. Adv Mater Technol 2018;3(12):1800136.
[159] Kunkel MH, Gebhardt A, Mpofu K, Kallweit S. Quality assurance in metal powder bed fusion via deep-learning-based image classification. Rapid Prototyping J 2019;26(2):259–66.
[160] Francis J, Bian L. Deep learning for distortion prediction in laser-based additive manufacturing using big data. Manuf Letters 2019;20:10–4.
[161] Ye D, Fuh YHJ, Zhang Y, Hong G, Zhu K. In situ monitoring of selective laser melting using plume and spatter signatures by deep belief networks. ISA Trans 2018;81:96–104.
[162] Mozaffar M, Paul A, Al-Bahrani R, Wolff S, Choudhary L, Agrawal A, Ehmann K, Cao J. Data-driven prediction of the high-dimensional thermal history in directed energy deposition processes via recurrent neural networks. Manuf Letters 2018;18:35–9.
[163] Bai Y, Yang Y, Xiao Z, Zhang M, Wang D. Process optimization and mechanical property evolution of alsimg0.75 by selective laser melting. Mater Des 2018;140:257–66.
[164] Kurzynowski T, Gruber K, Stopyra W, Kuźnicka B, Chlebus E. Correlation between process parameters, microstructure and properties of 316 L stainless steel processed by selective laser melting. Mat Sci Eng A-Struct 2018;718:64–73.
[165] Budding A, Vaneker THJ. New strategies for powder compaction in powder-based rapid prototyping techniques. Procedia CIRP 2013;6:527–32.
[166] Price S, Cooper K, Chou K. Evaluations of temperature measurements by near-infrared thermography in powder-based electron-beam additive manufacturing. In: Solid Free Fabr Symp Proc. 2012, p. 761–73.
[167] Yang HJ, Hwang PJ, Lee SH. A study on shrinkage compensation of the SLS process by using the taguchi method. Int J Mach Tool Manu 2002;42(11):1203–12.
[168] Buchbinder D, Meiners W, Pirch N, Wissenbach K. Investigation on reducing distortion by preheating during manufacture of aluminum components using selective laser melting. J Laser Appl 2014;26:012004.
[169] Farshidianfar MH, Khajepour A, Gerlich A. Real-time control of microstructure in laser additive manufacturing. Int J Adv Manuf Technol 2016;82:1173.
[170] Dai K, Shaw L. Distortion minimization of laser-processed components through control of laser scanning patterns. Rapid Prototyping J 2002;8(5):270–6.
[171] Kobryn P, Semiatin S. Microstructure and texture evolution during solidification processing of Ti–6Al–4V. J Mater Process Technol 2003;135:330–9.
[172] Song L, Bagavath-Singh V, Dutta B, Mazumder J. Control of melt pool temperature and deposition height during direct metal deposition process. Int J Adv Manufact Technol 2012;58:247–56.
[173] Song L, Mazumder J. Feedback control of melt pool temperature during laser cladding process. IEEE Trans Control Syst Technol 2011;19(6):1349–56.
[174] Bi G, Schurmann B, Gasser A, Poprawe R. Development and qualification of a novel laser-cladding head with integrated sensors. Int J Mach Tool Manu 2007;47(3):555–61.
[175] Hu D, Kovacevic R. Modeling and control for laser-based additive manufacturing. Int J Mach Tool Manu 2003;43(1):51–60.
[176] Salehi D, Brandt M. Melt pool temperature control using LabVIEW in Nd: YAG laser blown powder cladding process. Int J Adv Manuf Tech 2006;29(3):273–8.
[177] Tang L, Landers RG. Layer–to–layer height control for laser metal deposition processes. ASME J Manuf Sci Eng 2011;133(2):021009.
[178] Steuben JC, Birnbaum AJ, Iliopoulos AP, Michopoulos JG. Towards feedback control for additive manufacturing processes via enriched analytical solutions. J Comput Inf Sci Eng 2019;19(3):031009.
[179] Zheng C, Wen JT, Diagne M. Distributed temperature control in laser-based manufacturing. ASME J Dyn Sys Meas Control 2020;142(6):061001.

[180] Li J, Wang Q, Michaleris P, Reutzel EW, Nassar AR. An extended lumped parameter model of melt-pool geometry to predict part height for directed energy deposition. J Manuf Sci Eng 2017;139(9):091016.
[181] Wang Q, Michaleris P, Nassar AR, Irwin JE, Ren Y, Stutzman CB. Model-based feedforward control of laser powder bed fusion additive manufacturing. Addit Manuf 2020;31:100985.
[182] Fathi A, Khajepour A, Durali M, Toyserkani E. Geometry control of the deposited layer in a nonplanar laser cladding process using a variable structure controller. J Manuf Sci Eng 2008;130(3):031003.
[183] Cao X, Ayalew B. Robust multivariable predictive control for laser-aided powder deposition processes. J Franklin I 2019;356(5):2505–29.